

Factors Affecting the Evolution of Hurricane Erin (2001) and the Distributions of Hydrometeors: Role of Microphysical Processes

GREG M. MCFARQUHAR,* HENIAN ZHANG,* GERALD HEYMSFIELD,⁺ ROBBIE HOOD,[#] JIMY DUDHIA,[@]
JEFFREY B. HALVERSON,⁺ AND FRANK MARKS JR. &

**Department of Atmospheric Sciences, University of Illinois at Urbana-Champaign, Urbana, Illinois*

⁺*NASA Goddard Space Flight Center, Greenbelt, Maryland*

[#]*NASA Marshall Space Flight Center, Huntsville, Alabama*

[@]*National Center for Atmospheric Research, Boulder, Colorado*

& *NOAA/Hurricane Research Division, Miami, Florida*

(Manuscript received 11 November 2003, in final form 8 March 2005)

ABSTRACT

Fine-resolution simulations of Hurricane Erin are conducted using the fifth-generation Pennsylvania State University-NCAR Mesoscale Model (MM5) to investigate roles of thermodynamic, boundary layer, and microphysical processes on Erin's structure and evolution. Choice of boundary layer scheme has the biggest impact on simulations, with the minimum surface pressure (P_{\min}) averaged over the last 18 h (when Erin is relatively mature) varying by over 20 hPa. Over the same period, coefficients used to describe graupel fall speeds (V_g) affect P_{\min} by up to 7 hPa, almost equivalent to the maximum 9-hPa difference between microphysical parameterization schemes; faster V_g and schemes with more hydrometeor categories generally give lower P_{\min} . Compared to radar reflectivity factor (Z) observed by the NOAA P-3 lower fuselage radar and the NASA ER-2 Doppler radar (EDOP) in Erin, all simulations overpredict the normalized frequency of occurrence of Z larger than 40 dBZ and underpredict that between 20 and 40 dBZ near the surface; simulations overpredict Z larger than 25 to 30 dBZ and underpredict that between 15 and 25 or 30 dBZ near the melting layer, the upper limit depending on altitude. Brightness temperatures (T_b) computed from modeled fields at 37.1- and 85.5-GHz channels that respond to scattering by graupel-size ice show enhanced scattering, mainly due to graupel, compared to observations. Simulated graupel mixing ratios are about 10 times larger than values observed in other hurricanes. For the control run at 6.5 km averaged over the last 18 simulated hours, Doppler velocities computed from modeled fields (V_{dop}) greater than 5 m s^{-1} make up 12% of Erin's simulated area for the base simulation but less than 2% of the observed area. In the eyewall, 5% of model updrafts above 9 km are stronger than 10 m s^{-1} , whereas statistics from other hurricanes show that 5% of updrafts are stronger than only 5 m s^{-1} . Variations in distributions of Z , vertical motion, and graupel mixing ratios between schemes are not sufficient to explain systematic offsets between observations and models. A new iterative condensation scheme, used with the Reisner mixed-phase microphysics scheme, limits unphysical increases of equivalent potential temperature associated with many condensation schemes and reduces the frequency of Z larger than 50 dBZ, but has minimal effect on Z below 50 dBZ, which represent 95% of the modeled hurricane rain area. However, the new scheme changes the Erin simulations in that 95% of the updrafts are weaker than 5 m s^{-1} and P_{\min} is up to 12 hPa higher over the last 18 simulated hours.

1. Introduction

Quantitative precipitation forecasts (QPFs) require knowledge of synoptic, mesoscale, and microscale processes, and an adequate representation of these pro-

cesses in models. To improve QPFs for hurricanes, improved knowledge of cloud microphysical, thermodynamic, and turbulent processes; land surface-atmosphere interactions; improved measurements of atmospheric water vapor; a better understanding of mesoscale dynamics; and further development of mesoscale numerical models and cumulus parameterization schemes are required. Although several studies have investigated the influence of many such processes on the evolution of hurricanes, fewer recent studies have

Corresponding author address: Prof. Greg M. McFarquhar, Dept. of Atmospheric Sciences, University of Illinois at Urbana-Champaign, 105 S. Gregory Street, Urbana, IL 61801.
E-mail: mcfarq@atmos.uiuc.edu

examined the impacts of cloud microphysical processes on the structure and evolution of these systems and on their QPFs.

Previous studies showed that representations of microphysical processes affect simulations of hurricanes. Willoughby et al. (1984) showed that hurricane simulations with parameterized ice microphysics had a different structure and evolution compared to those with liquid water microphysics. Lord et al. (1984) and Lord and Lord (1988) used an axisymmetric, nonhydrostatic model to show that cooling associated with melting ice particles initiates and maintains model downdrafts, the extent and intensity of which are determined by horizontal advection of hydrometeors from convection together with fall speeds of snow and graupel. The downdrafts contribute to the formation of multiple convective rings that in turn modify storm development (Willoughby et al. 1984). McCumber et al. (1991) evaluated the performance of several ice parameterizations in both tropical squall-type and nonsquall-type systems, concluding that their simulations were more strongly influenced by differences in descriptive microphysical parameters (e.g., size distribution intercept parameter and particle density) than by differences in the way microphysical processes were treated in the ice schemes. They suggested that the application of bulk ice microphysics in cloud models might be case specific, indicating that microphysical sensitivity studies for other cloud systems may not apply to hurricanes. Uncertainties associated with microphysics must also be placed in the context of uncertainties associated with other processes.

Other studies have focused on how initial conditions, rainfall assimilation, and cumulus parameterization schemes (Karyampudi et al. 1998), boundary layer schemes (Braun and Tao 2000), and the role of a gradient of angular momentum above regions of maximum convective heating (Krishnamurti et al. 1998) affect hurricane simulations. Simulations with high resolution (Liu et al. 1997, 1999) showed that the track, intensity, and inner-core structures of Hurricane Andrew could be reproduced using realistic model physics and proper initial vortices. Liu et al. (1997) also suggested that the axisymmetric models used in earlier studies did not adequately represent storm–environment interactions, suggesting previous microphysical sensitivity studies using axisymmetric models might not be applicable. Rogers et al. (2004) also report on the sensitivity of hurricane processes to the representations of microphysics.

In this paper, simulations of Hurricane Erin 2001, conducted using the fifth-generation Pennsylvania State University–National Center for Atmospheric Research (PSU–NCAR) Mesoscale Model (MM5, version

3.5), are used to examine impacts of boundary layer and microphysical parameterization schemes on the growth and maintenance of Erin. Impacts of varying coefficients that describe the fall velocities of graupel particles on hurricane dynamics are described. A new iterative condensation scheme, developed here to limit the artificial increase of equivalent potential temperature Θ_e that occurs during the adjustment step of many condensation schemes (Bryan and Fritsch 2000) is also tested.

Observations made on 10 September 2001 during flights of the National Aeronautics and Space Administration (NASA) ER-2 and National Oceanic and Atmospheric Administration (NOAA) P-3 aircraft during the Fourth Convection and Moisture Experiment (CAMEX-4) provide a framework for interpretation of model results. Vertical profiles of radar reflectivity factor (Z) and Doppler velocity (V_{dop}) obtained from the ER-2 Doppler radar (EDOP; Heymsfield et al. 1996) are compared against Z and V_{dop} derived from modeled fields. Distributions of Z observed by the P-3 lower fuselage radar are also compared against modeled fields. Brightness temperatures (T_b) measured at four frequencies by the Advanced Microwave Precipitation Radiometer (AMPR; Spencer et al. 1994) on the ER-2 are compared with T_b calculated using modeled hydrometeor fields as input to a microwave radiative transfer model (C. Kummerow 2004, personal communication). Temperature T and moisture q_v profiles from dropsondes released in the eye are compared against modeled profiles to determine their sensitivity to the condensation scheme. Modeled fields are also compared against updraft and downdraft statistics observed in other hurricanes (Black et al. 1996) and against graupel mixing ratios estimated from in situ observations in other storms (McFarquhar and Black 2004).

The remainder of this paper is organized as follows. Section 2 provides information on the structure and evolution of Erin based on observations acquired during CAMEX-4, concentrating on those observations used to assess the simulations and sensitivity studies outlined in section 3. Section 4 describes simulation results and impacts of microphysical, thermodynamic, and boundary layer processes on the structure and evolution of Erin. The significance of the results is summarized in section 5.

2. Observations of Hurricane Erin

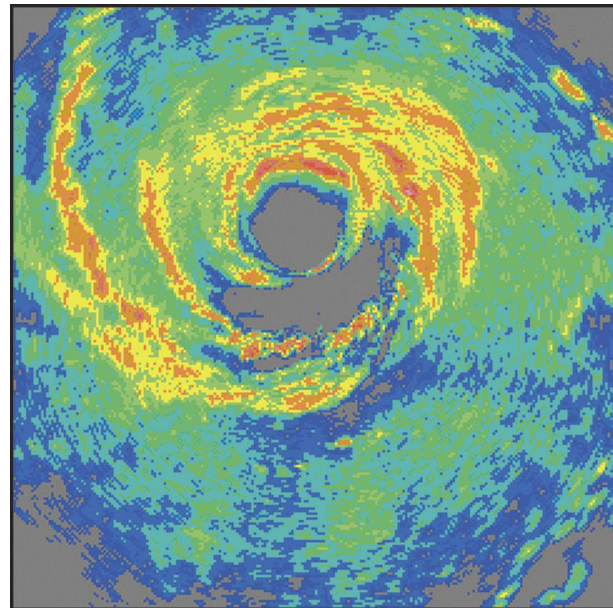
Hurricane Erin (2001) was the first tropical cyclone in the Atlantic Ocean Basin to reach hurricane status in 2001 and achieved maximum wind speeds of approximately 54 m s^{-1} . Pasch and Brown (2002) report that

Erin formed from a tropical wave emerging over West Africa and weakened and strengthened a number of times before regaining tropical storm strength on 7 September 2001. After brushing Bermuda on 9 September, Erin moved to the north-northwest and weakened more slowly than typical storms (Pasch and Brown 2002). Erin reached category 3 on the Saffir–Simpson scale and never made landfall. Erin is a good candidate for studies of microphysical effects on storm evolution because additional unknowns about impacts of landfall are avoided. However, possible impacts of land-based aerosols such as African dusts and urban pollutants on the microphysics may be present because appreciable cloud condensation nuclei were measured in the eye (Hudson and Simpson 2002).

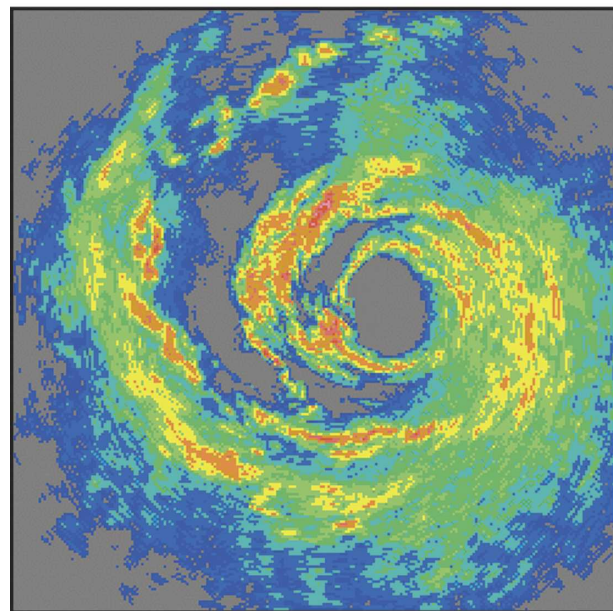
Observations of Erin are plentiful. During CAMEX-4, the NOAA P-3 and the NASA ER-2 and DC-8 aircraft flew in coordination obtaining comprehensive data on the wind, T and q_w structures on 10 September 2001. The observations were made when Erin was beginning to decay with the maximum winds dropping by 12.5 m s^{-1} during the flight of the NOAA P-3. In addition, the warm core was weakening from top down and the eyewall convection became much shallower during the course of the ER-2 aircraft observations (Halverson et al. 2006). These observations still offer a great opportunity to study and evaluate feedbacks between microphysics and dynamics.

Figure 1a shows an image of Erin obtained 10 September 2001 from a sweep of the lower fuselage radar during the first penetration of the P-3 into Erin at 1811:54 UTC at an altitude of 4.2 km near the freezing level. Depending on time and the threshold Z used to define the eye, its diameter varies between 30 and 60 km with the diameter sometimes hard to define given the clear wavenumber-1 asymmetry in the inner eyewall. A time series of images shows that the weak rain portion of this asymmetry rotates counter clockwise, being south of the eye in Fig. 1a and west of it during the second penetration at 1914:16 UTC as shown in Fig. 1b. Aberson et al. (2006) and Wu et al. (2006) characterize this asymmetry and hypothesize causes for its existence. Other asymmetries in Z were noted, with rainbands of maximum Z to the north and east of the eye at 1811:54 UTC and to the west and south at 1914:16 UTC.

The maximum Z for Erin at the time of these observations is approximately 45–46 dBZ and the overall storm diameter about 360 km. The spacing, width, and length of the asymmetrical rainbands varies with time, but typical values are on the order of 20 km for spacing, 10 km for width, and 50 km for length. Following Fig. 3.4 of Doviak and Zrnich (1984), it is estimated that



(a)



(b)

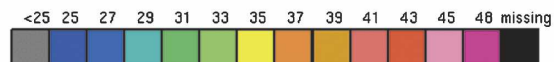


FIG. 1. Radar reflectivity Z obtained from lower fuselage radar on board NOAA P-3 aircraft during first and second penetrations through Hurricane Erin at 1811:24 and 1913:46 UTC.

a 40-dBZ rainband would be attenuated at a rate of $0.018 \text{ dBZ km}^{-1}$ for a 5-cm radar. Thus, for the most intense rainbands Z would be attenuated by about 0.36 dBZ assuming a 10-km width.

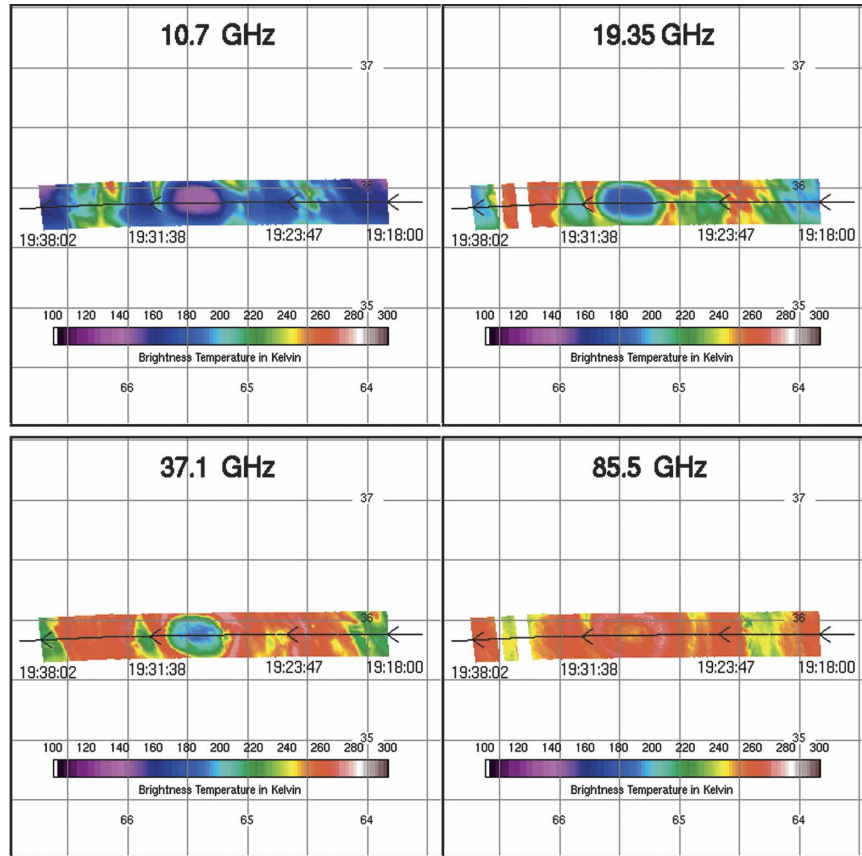


FIG. 2. Brightness temperature T_b is measured by AMPR at 10.7, 19.35, 37.1, and 85.5 GHz for the transect that the NASA ER-2 flew over the eye of Erin between 1918:00 and 1938:02 UTC.

Figure 2 shows brightness temperatures (T_b) measured at 10.7, 19.35, 37.1, and 85.5 GHz by AMPR over Erin's eye between 1916:20 and 1938:14 UTC. The spatial resolution of these observations at a flying altitude of 20 km is 0.6 km at 85.5 GHz, 1.5 km at 37.1 GHz, and 2.8 km at 19.35 and 10.7 GHz. The eye is indicated by radiometrically colder T_b of around 140 K at 10.7 GHz and of around 180 K at 19.35 and 37.1 GHz. At 85.5 GHz, water vapor emission causes the clear eye to have higher a T_b between 220 and 250 K. Lower T_b noted for all channels near the eye's center compared to regions closer to the eyewall is caused by lower vapor emission, suggesting drying. By comparing similar AMPR images for other transects over the eye, the eye is seen to move to the northeast at approximately 8 m s^{-1} during the 3-h period (1648:59 to 1950:30 UTC) of the observations. The eye's diameter is estimated at 37 km from the 10.7-, 19.35-, and 37.1-GHz channels similar to that estimated with the P-3 radar. The horizontal dimension of the storm is approximately 300 km, determined by looking at emissions in the lower three frequency channels and scattering at the highest frequency.

Emission from heavy rain associated with the eyewall

and outer rainbands corresponds to regions of warmer T_b of around 240 K at 10.7 and of around 260 K at 19.35 GHz. Regions of T_b at 37.1 GHz around 220 K between 65.7° and 65.8°W and between 64.7° and 64.8°W likely correspond to the ocean surface as coincident EDOP data from the same time (Fig. 3) show lower Z or rain free regions. There is a small region of T_b below about 240 K around 64.4°W that is consistent with a scattering signature from precipitation-sized ice or graupel as it corresponds to the major rainband in the EDOP data at 300 km (Fig. 3). Regions of T_b in the range from 220 to 240 K at 85.5 GHz between 66° and 66.5°W , between 64° and 64.5°W and in narrow bands 10 to 20 km wide at 65.7° and 64.9°W are due to scattering from some combination of small, low-density ice, large snowflakes, and graupel. Since supercooled water can have different effects on scattering in the 37.1- and 85.5-GHz channels (Cecil and Zipser 2002), if it were present, it would also impact data interpretation. In general, scattering effects at 37.1- and 85.5-GHz channels are much less than those associated with a squall line over the Gulf of Mexico (Spencer et al. 1994) suggesting that even though graupel-size ice is present in Erin, large

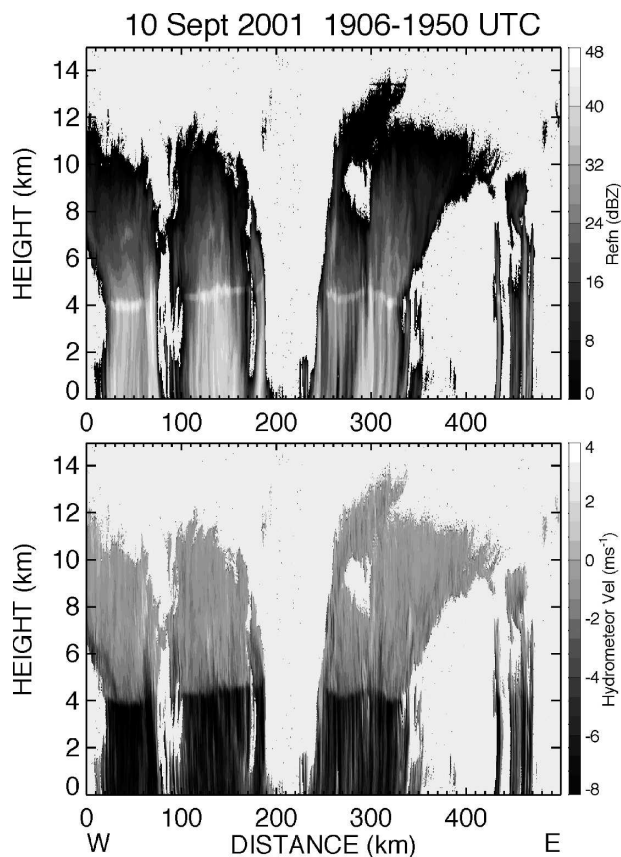


FIG. 3. Here, Z and V_{dop} , a combination of ambient velocity and particle fall speed, are obtained by EDOP for transect flown to the west and shown in Figs. 1b and 2.

amounts are not needed to explain AMPR observations. Since there is some ambiguity in interpreting AMPR scattering behavior, T_b predicted using modeled fields as input to a radiative transfer model are compared against observations in section 5.

Vertical profiles of V_{dop} , a combination of ambient velocity and particle fall speed, and Z derived from downward-pointing EDOP data are shown for the same time period in Fig. 3. The rate of attenuation for Z at 9.6 GHz is approximately $5.6 \times 10^5 \exp(0.2Z)$ (Doviak and Zrnic 1984). Thus, for the intense rainbands of approximately 40 dBZ the two-way attenuation is about 2 dBZ over a 50-km depth. To the west of the 40–50-km-wide eye, the rainbands are more intense with two regions of precipitation of varying intensity each about 60 km wide seen. In contrast the inner eyewall is only about 7 km wide. To the east both the eyewall and outer layers are less intense and broad. Although there is no substantial tilting of the eyewall below the melting layer, tilting is seen above the melting layer at distance labels of 180 and 240 km in Fig. 3. For example, on the east side the inner eyewall edge appears to slope 10–15

km over a depth from 6 to 8 km with a much reduced slope below the melting layer. Earlier transects flown from the southwest to the northeast and from the northwest to southeast showed greater tilting on the northeast and northwest side of the eye, respectively (Halverson et al. 2006). Combined, these data suggest a northward tilt of the vortex consistent with Wu et al. (2006). Wu et al. (2006) showed that changes in the vortex tilt, combined with changes in storm-relative asymmetric flow, could be used to explain observed changes in Erin's precipitation structure. A bright band is noted about 4–4.5 km above the surface and considerable small-scale structure is seen at all levels. The increase in V_{dop} below the bright band compared to that above is associated with an increase in particle fall speed as snow particles melt to raindrops.

Dropsondes released from the ER-2 over the eye and rainbands give temperature measurements within $\pm 0.2^\circ\text{C}$ and water vapor and wind speeds within 2%. One dropsonde was released in the eye, two near the eyewall, and five in the outer peripheries of the storm. Halverson et al. (2006) show that substantial drying and extremely low humidity are found within the eye between 2 and 10 km, with dewpoint depressions between 15 and 30 K, much larger than for the ambient environment outside the hurricane. Weak horizontal winds of approximately 10 m s^{-1} were also noted.

In addition to observations from Erin, past studies provide information on distributions of parameters in other hurricanes. For example, when analyzing vertical motion characteristics of seven tropical cyclones, Black et al. (1996) found the broadest distribution of vertical motion in the eyewall where 5% of the motions were greater than 5 m s^{-1} . Doppler updrafts greater than 1 m s^{-1} accounted for less than 30% of the area but greater than 75% of the upward mass flux; similarly, downdrafts greater than 1 m s^{-1} accounted for 10% of the area and about 50% of the downward mass flux. Using in situ data collected by the NOAA P-3, McFarquhar and Black (2004) found graupel mass concentrations greater than 0.5 g m^{-3} were only infrequently observed near the melting layer.

The above data provide information about horizontal dimensions, eye sizes, frequency distributions of Z , V_{dop} , graupel and updrafts/downdrafts, microwave T_b , and thermodynamic profiles for Erin that should be statistically replicated by simulations. The properties include smaller amounts of graupel aloft than found in midlatitude storms, maximum Z of approximately 40–45 dBZ, a deep dry layer in the eye, highly asymmetric and variable distributions of precipitation, 95% of updrafts less than 5 m s^{-1} , eye dimensions of 30–40 km, and horizontal dimensions on the order of 400 km.

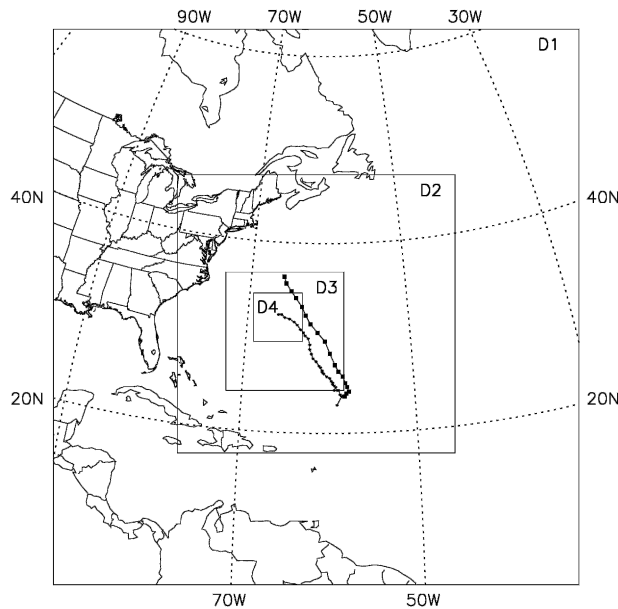


FIG. 4. Domain used in MM5 base simulations of Hurricane Erin. Outer grid has horizontal resolution of 54 km, inner grids have resolutions of 18, 6, and 2 km. All domains have two-way nesting except coarse domain. Line with large dots represents observed track of Erin, whereas line with smaller dots represents track of Erin produced by base simulation.

3. Model simulations

A series of numerical simulations of Hurricane Erin were conducted using MM5 (Grell et al. 1995), a limited-area, nonhydrostatic, sigma (σ)-coordinate model designed to simulate or predict mesoscale atmospheric circulations. Simulations describe a 4-day period from 0000 UTC 7 September 2001 to 0000 UTC 11 September 2001. During this time the observed central pressure of Hurricane Erin dropped from 1012 to 968 hPa (at 1800 UTC 9 September 2001) and then rose back to 973 hPa (Pasch and Brown 2002). Figure 4 shows the

coarse- and fine-mesh domains used for the control simulation consisting of 112 by 112 grid points in x , y with a grid spacing of 54 km. Higher-resolution simulations were performed for three finer grids of 18, 6, and 2 km. All domains had two-way nesting except for the coarse domain. The numbers of grid points in the inner domains are 181 by 181 (18 km), 226 by 226 (6 km), and 280 by 280 (2 km). Because of computational expense, the finer-resolution domains were used only when Erin had started to intensify, with the 6-km domain initialized at 1200 UTC 9 September and the 2-km domain initialized at 0000 UTC 10 September. There are 36 uneven σ levels or 35 half- σ levels in the vertical, with the surface pressure and 20 hPa being the pressures at the surface and model top. The innermost domain was moved 3–4 times, depending upon the simulation, to keep the hurricane eye nearly centered in the fine domain. The Betts–Miller convective scheme was used in the three coarser meshes, but was excluded in the inner 2-km domain. Table 1 summarizes the other physics options used for the control simulation including the Goddard cloud microphysics and the Burk–Thompson (1989) boundary layer scheme.

Temperature, humidity, geopotential height, and winds from the National Centers for Environmental Prediction (NCEP) global analyses on 1° by 1° grids were used for the initial and boundary conditions. Analysis products were interpolated to model grid points and σ levels. When the surface wind and temperature fields were grid-nudged toward the analysis for the first 6 h of the simulation, improvements in simulated track and minimum sea level pressure P_{\min} were not produced. Simulations that started at other times or used analyses from the European Centre for Medium-Range Weather Forecasts (ECMWF) did not give as good an agreement with observations and sometimes it was difficult to get a storm to intensify under such conditions. Although reasons for differences be-

TABLE 1. Summary of different series of simulations performed. All simulations had 35 half- σ levels and 2-km horizontal resolution within the fine D4 domain. No convective parameterization scheme was used in domain D4, and the Betts–Miller scheme was used for domains D1–D3.

Series	Simulations performed	Other conditions
Microphysical parameterization scheme	Goddard microphysics, Reisner mixed phase, simple ice	Burk–Thompson scheme and Eta scheme used in separate simulation series
Boundary layer parameterization scheme	Blackadar Eta Burk–Thompson	Goddard microphysics
Graupel fall speed representation	$(a_g, b_g) = (351.2 \text{ cm}^{0.63} \text{ s}^{-1}, 0.37)$ base $(199.9 \text{ cm}^{0.75} \text{ s}^{-1}, 0.25), (700.1 \text{ cm}^{0.25} \text{ s}^{-1}, 0.75)$	Goddard microphysics Burk–Thompson planetary boundary layer scheme
Thermodynamic scheme	Usual condensation scheme New condensation scheme	Reisner mixed-phase microphysics Burk–Thompson PBL scheme

tween these simulations are no doubt important, this study concentrates on model sensitivities to parameterized physical processes.

Simulations are conducted with varying boundary layer, microphysical, and thermodynamic schemes to investigate the roles of such processes in the growth and maintenance of Erin. Table 1 summarizes the sensitivity experiments. All simulations involve application of preexisting parameterization schemes with two exceptions. First, a thermodynamic test involves the use of a new iterative condensation scheme, described in the appendix, which limits the unphysical increase of Θ_e associated with many existing condensation schemes. The development of this scheme was motivated by Bryan and Fritsch (2000), who determined that unrealistically high values of Θ_e were predicted in numerical models for rapidly growing updrafts in highly convectively unstable midlatitude thunderstorms because of the manner in which time integration is performed and because of the way in which condensation is treated. The new scheme limits this artificial increase in T and q_w . It was unknown prior to our simulations whether these artificial increase would have large impacts on hurricane simulations since maximum hurricane updrafts of about 10 m s^{-1} are substantially lower than updrafts of 50 m s^{-1} that occur in the midlatitude thunderstorms simulated by Bryan and Fritsch (2000).

Another series of simulations examines the dependence on descriptive microphysical parameters and, in particular, on coefficients used to describe graupel fall speeds V_g . The role of graupel is a key focus because of the importance of graupel conversion processes in latent heat release and storm dynamics (e.g., Lord and Lord 1988). McFarquhar and Black (2004) identified a range of a/b coefficients, where $V = aD^b$, that apply to graupel. From their Fig. 3 and as shown in Table 1, coefficients corresponding to faster and slower falling graupel are used in simulations.

Section 4 describes simulation results, placing uncertainties associated with the use of microphysics in the context of uncertainties associated with other schemes. Although most fields are directly output by MM5, Z must be calculated from modeled mass mixing ratios of graupel (q_g), snow (q_s), and rain (q_r) following

$$Z = N_{0r}^*(\rho_a q_r)^{7/4} + \alpha N_{0g}^*(\rho_a q_g)^{7/4} + \alpha N_{0s}^*(\rho_a q_s)^{7/4}, \quad (1)$$

where ρ_a is the density of air, α is a factor of 0.224 that accounts for the different dielectric constants of water and ice (Smith 1984), and N_{0r}^* , N_{0g}^* , and N_{0s}^* are related to the respective intercept parameters for rain (N_{0r}), graupel (N_{0g}), and snow (N_{0s}) through the relation of Stoelinga (2005):

$$N_{0(r,s,g)}^* = \frac{\Gamma(7)}{(\pi \rho_{(r,s,g)} \Gamma(4)/6)^{7/4}} \left(\frac{\rho_{(r,s,g)}}{\rho_r} \right)^2 N_{0(r,s,g)}^{-3/4}, \quad (2)$$

where $\rho_{r,s,g}$ represents the density of either rain, snow, or graupel.

4. Model results

a. Storm tracks

The simulated tracks of Erin vary by at most 57 km for simulations described in Table 1. Figure 4 shows the track of Erin for the control simulation. All simulated tracks were consistently west of the observed track with the amount of westward shift varying by between 18 and 57 km for different simulations. At 0000 UTC 11 September, the simulated Erin was moving at 6 m s^{-1} to the north-northwest, a bit slower than the 8 m s^{-1} observed. The use of different domains, large-scale initial conditions, and initialization times failed to yield better tracks that also produced reasonable P_{\min} for all simulations. Variations in the representation of physical processes had substantial impacts on P_{\min} and on predicted wind speeds as discussed below; however, changes in the predicted track by amounts greater than 57 km only occurred when using different large-scale initial conditions and not when using different representations of physical processes. Hence, it is concluded that the large-scale flow is largely responsible for determining storm track.

b. Predicted sea level pressures and surface winds

Figure 5 shows the temporal variation of P_{\min} and maximum surface wind speed (U_{\max}) for simulations using the Burk–Thompson (1989) boundary layer scheme and three microphysical schemes. The lines in Fig. 6 represent similar simulations except that the Eta scheme characterizes boundary layer processes. Although all simulations in Fig. 5 exhibit a quicker intensification between 1200 UTC 7 September and 0000 UTC 9 September than do observations, P_{\min} averaged over the last 18 h differs by only 5 hPa from observations. However, differences up to 15 m s^{-1} from observed surface winds are noted and the model does not represent the decline in winds seen in the last 18 h. For the Eta simulations (Fig. 6), there is larger variation between microphysical schemes in how quickly Erin intensifies and in that P_{\min} averaged over the last 18 h varies by 9 hPa. This shows no simple relationship between use of specific microphysical schemes and cyclone intensity exists and that the impact of different schemes may depend on the choice of boundary layer or other schemes.

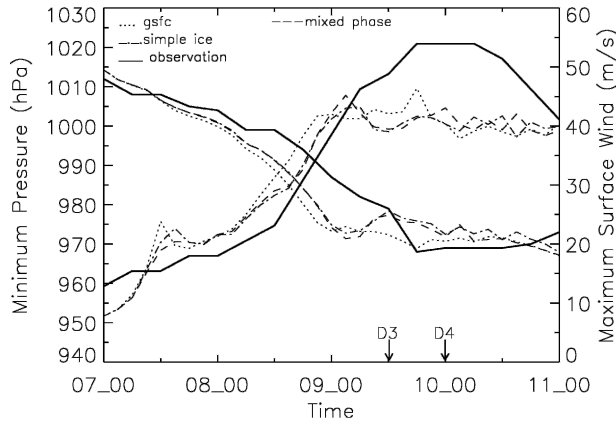


FIG. 5. Temporal evolution of P_{\min} and U_{\max} between 0000 UTC 7 Sep 2001 and 0000 UTC 11 Sep 2001. Solid lines represent observations, different line types correspond to simulations conducted with varying microphysical parameterization schemes as indicated in legend; all simulations use the Burk–Thompson boundary layer scheme. Here, D3 (D4) indicates the time at which 6-km (2 km) grid is activated. See Table 1 for description of other base simulation conditions. On the left side of the plot, lower lines refer to wind and upper lines refer to pressure.

The microphysical schemes differ in complexity and in how many hydrometeor species are included. The simple ice scheme of Dudhia (1989), which allows only ice above the melting layer and water below, is less detailed than the Reisner et al. (1998) mixed-phase scheme, which allows ice and snow, but no graupel or riming processes. The Goddard microphysics scheme (Lin et al. 1983; Tao and Simpson 1993) adds equations for the prediction of graupel. The Reisner graupel scheme was not used in this series of simulations. In general, as more details and species are included, Erin intensifies to lower P_{\min} and greater U_{\max} ; for example, the Goddard scheme gives lower P_{\min} for most times in

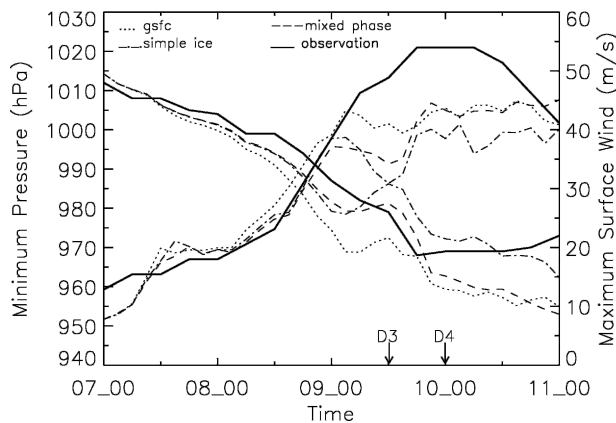


FIG. 6. As in Fig. 5, except for different microphysical simulations conducted using the Eta boundary layer scheme.

Figs. 5 and 6, whereas the simple ice scheme typically gives higher P_{\min} . There are exceptions to this trend; in Fig. 6 the use of the mixed-phase scheme produces lower P_{\min} at the end of the simulation than does the Goddard scheme. Mutual interactions between physical parameterizations can make the impact of a given physical process less clear.

Previous studies for midlatitude convective systems (McCumber et al. 1991) have shown that not only does the choice of microphysics scheme affect results, but also the choice of descriptive microphysical parameters, such as the intercept of the size distributions and hydrometeor fall velocities. Figure 7 shows how P_{\min} and U_{\max} vary with time for simulations with varying representations of V_g in the Goddard scheme. For different simulations, P_{\min} and U_{\max} start to diverge after Erin has intensified (0900 UTC 9 September) and just before the fine domain simulations are initialized (D3 and D4). Differences of 7 hPa in P_{\min} and 5 m s^{-1} in U_{\max} between simulations are noted when averaged over the last 18 h. This variation between P_{\min} and U_{\max} is comparable to that seen using different microphysics schemes. Simulations with faster V_g consistently produce lower P_{\min} and faster U_{\max} compared to those with slower V_g . Because various microphysics schemes have different descriptive parameters, it is hard to decouple effects associated with varying schemes and microphysical parameters. Nevertheless, Fig. 7 shows that even the representation of one descriptive parameter can impact simulations.

To place uncertainties associated with representations of microphysics in context, Fig. 8 shows how the representation of the boundary layer affects P_{\min} and U_{\max} where all simulations are conducted with God-

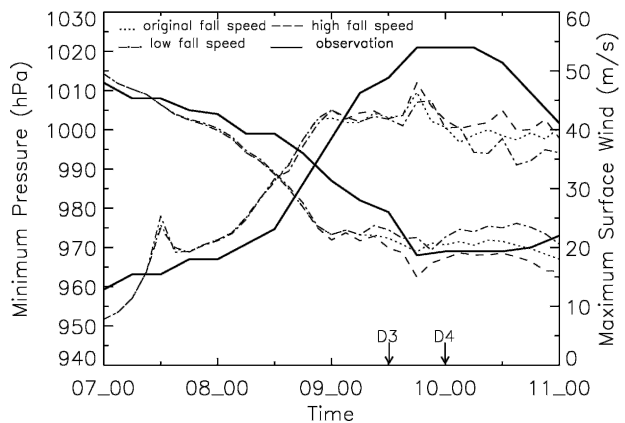


FIG. 7. As in Fig. 5, except for different choice of (a_g, b_g) coefficients that describe fall velocity of individual graupel particles within the Goddard microphysics scheme. Coefficients corresponding to different fall velocities are fast ($700.1 \text{ cm}^{0.75} \text{ s}^{-1}$, 0.37); medium ($351.2 \text{ cm}^{0.63} \text{ s}^{-1}$, 0.37); and slow ($199.9 \text{ cm}^{0.75} \text{ s}^{-1}$, 0.25).

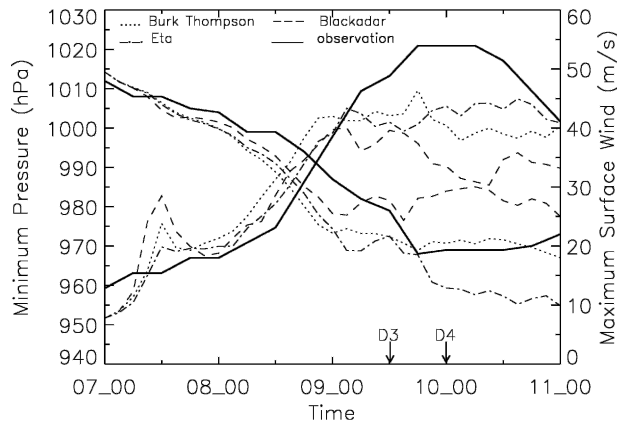


FIG. 8. As in Fig. 5, except for simulations with different boundary layer schemes as indicated in the legend.

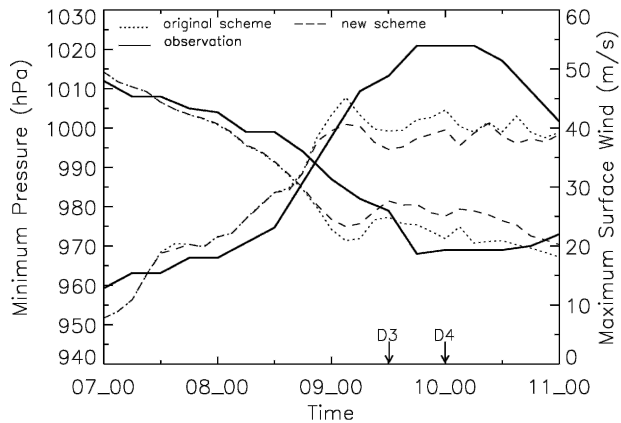


FIG. 9. As in Fig. 5, except different line types correspond to use of existing condensation scheme or new iterative condensation scheme as described in legend.

dard microphysics. Although the schemes initially give similar results, they start to diverge at 0300 UTC 9 September after Erin has intensified to 983 hPa and diverge even more when the fine domains are initialized. Differences between simulations are greater than those with varying microphysics: P_{\min} averaged over the last 18 h varies by over 20 hPa and U_{\max} by up to 10 m s^{-1} , compared to differences of up to 9 hPa and 5 m s^{-1} for microphysics. The Burk–Thompson (1989) and Eta schemes compare best against observations for this combination of parameterizations. In general, the Blackadar scheme produces higher P_{\min} . Although detailed investigations of the physical mechanisms by which varying boundary layer schemes give larger U_{\max} and lower P_{\min} is beyond the scope of this paper, prior studies (Braun and Tao 2000) have shown that exchange coefficients for enthalpy C_k and momentum C_D play a major role.

The final simulation series looks at how a new representation of condensation affects Erin’s evolution to see if potential overestimates of heating and moistening associated with conventional schemes provide artificial warming, condensate production, and stronger updrafts to the degree that occurs in simulations of vigorous thunderstorms (Bryan and Fritsch 2000). Figure 9 shows the impact of the new condensation scheme on P_{\min} and U_{\max} for simulations using the Burk–Thompson (1989) boundary and Reisner et al. mixed-phase scheme. For averages over the last 18 h of Erin’s simulations, higher P_{\min} of 8 hPa and lower U_{\max} of 5 m s^{-1} are realized with the new condensation scheme, uncertainties comparable to those associated with representations of microphysics. For simulations with the Eta boundary scheme, the differences in P_{\min} and U_{\max} were even greater, with average differences of 12 hPa and 6 m s^{-1} (figure not shown). The new scheme re-

duces the condensation and associated latent heat release, thereby reducing the upper-level warming in the core and hydrostatically increasing the surface pressure.

The results presented in this subsection show that although the choice of microphysical parameterization scheme affects Erin’s strength, complex interactions between multiple processes must be considered to understand its strength and evolution. There is no easy interpretation of results or choice of correct parameterization scheme as microphysical schemes that produce results closest to observations for one boundary layer scheme, may not do so. Further, variation of only one free coefficient in the microphysical schemes can impact Erin’s simulation.

c. Impacts on hydrometeor distribution within hurricane

In this subsection, a quantitative analysis of how microphysical and thermodynamic processes affect horizontal and vertical distributions of hydrometeors is made by examining fields in addition to P_{\min} and U_{\max} . In addition to comparing simulated distributions against the Erin observations, comparisons with frequency distributions from prior studies of Black et al. (1996), Yuter and Houze (1995), Marks (1985), and McFarquhar and Black (2004) are made.

Figure 10 shows surface Z estimated using Eq. (1) for the microphysical schemes depicted in Fig. 5. The simulated hurricane eye ranges in size from 50 to 80 km and is between 25% and 100% larger than observed. The diameter of the region over which Z is distributed ranges from 250 to 400 km within the range of 300 km estimated from AMPR and EDOP. The model predicts asymmetrical distributions of Z consistent with obser-

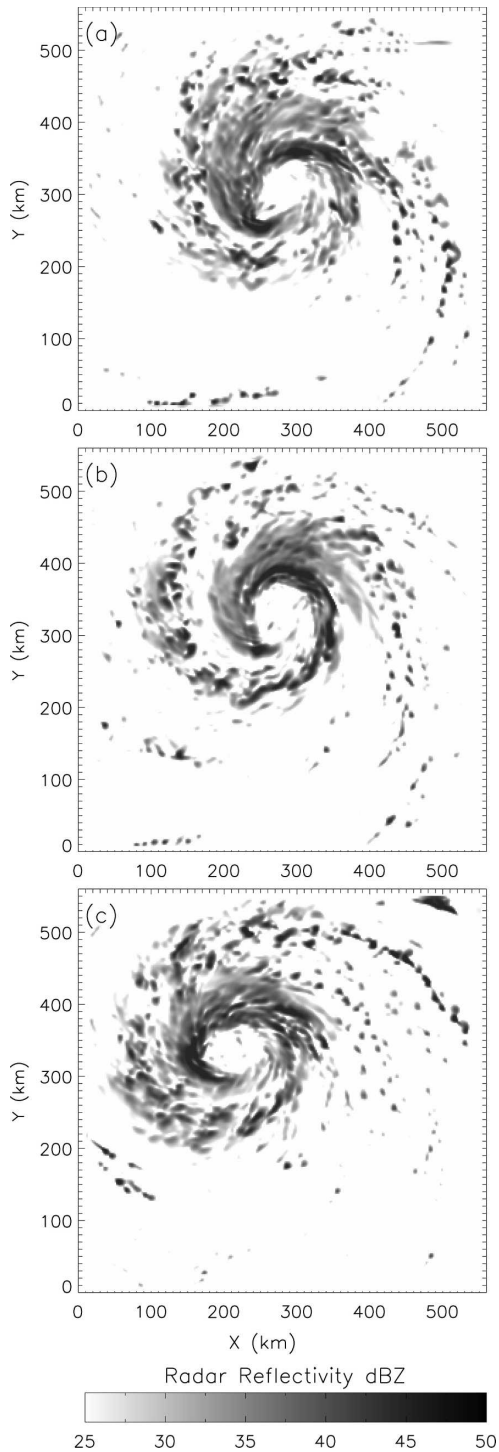


FIG. 10. Horizontal distribution of surface Z in inner domain at 0000 UTC 11 Sep 2001 for simulations using various microphysical schemes: (a) simple ice, (b) Reisner et al. (1998) mixed phase, and (c) Goddard microphysics.

vations. Typical rainband widths (12 km) compare reasonably with observed values of about 10 km. Differences in horizontal distributions are noted with regions of maximum Z to the north and south of the eye in the simple ice and Reisner simulations and to the west in the Goddard simulations at 0000 UTC 11 September.

Because minor differences in simulations can cause different temporal evolutions that affect the spatial distributions of Z , comparing horizontal Z patterns at specific times might not be meaningful. Instead statistical comparisons between frequency distributions of parameters from different simulations and observations are performed using a long averaging period. An 18-h period between 0600 UTC 10 September and 0000 UTC September 11 is chosen to cover the period in the simulations when Erin is mature (no major variation in P_{\min}), yet avoiding the first 6 h after D4 is initialized so that finescale processes will have had time to feed back on dynamics. The observations used to plot the frequency distributions are determined using data from all three sorties of the ER-2 over Erin for similar height levels as the simulations.

For simulations using varying microphysical parameterizations, Fig. 11 shows that the maximum simulated Z near the surface and for four levels with altitudes of 6.5, 5.6, 5.1, and 4.7 km, corresponding to average temperatures of -11° , -4° , -1° , and 0°C , are approximately 50 dBZ. This is larger than the maximum Z observed by the P-3 radar (Fig. 1) and by EDOP (Fig. 2). Attenuation on the order of 3 dBZ for the P-3 radar and 2 dBZ for EDOP (section 2) cannot explain the discrepancy.

Figure 12 shows a similar comparison where modeled Z comes from simulations using the new and original condensation scheme. For all simulations and levels, including those close to the surface, the model overpredicts the normalized frequency of occurrence of Z larger than about 35 dBZ but underpredicts that between 10 and 35 dBZ. The fact that observed echoes between 40 and 50 dBZ always contribute to less than 2% of the observed hurricane area may be dependent upon the fact that observations were made when U_{\max} and the storm were starting to decay: Yuter and Houze (1995) showed the frequency of occurrence of such high Z for a line of thunderstorms in Florida was strongly dependent on development stage. On the other hand, Black et al. (1996) also showed that echoes between 40 and 50 dBZ contributed less than 2% to area from seven Atlantic hurricanes.

Although the new iterative condensation scheme reduces the frequency of Z greater than 50 dBZ, such intense Z represent less than 5% of the storm area or approximately 1440 km^2 of area. A Mann–Whitney U

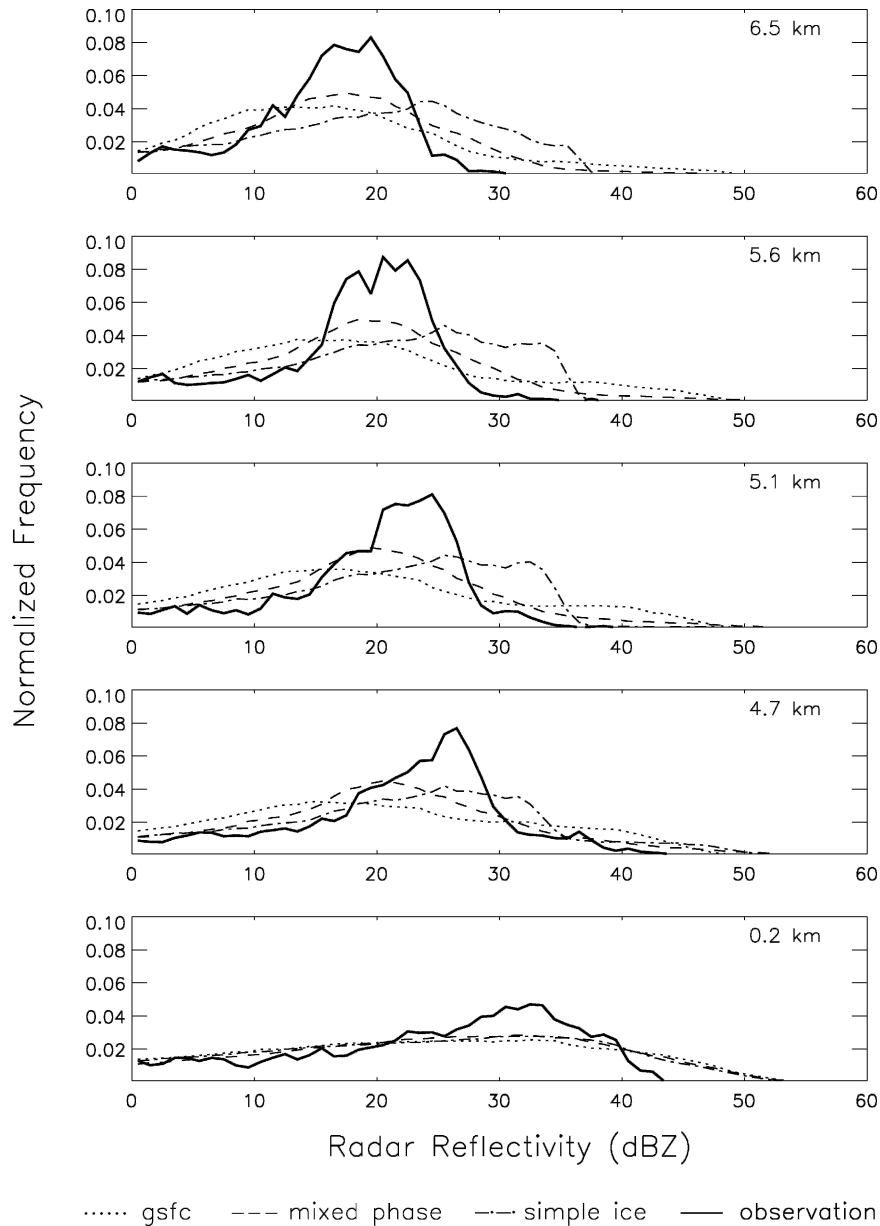


FIG. 11. Histogram of Z derived from EDOP (solid line) and from modeled fields at five indicated altitudes for simulations using different microphysical parameterization schemes as indicated in legend; Z histograms computed from modeled fields from last 18 h of simulation, and observations correspond to data collected during all three ER-2 sorties over Erin.

test (Vernoy and Kyle 2002), which determines whether two samples have the same mean without making a distribution assumption, is used to examine differences between means. Even with the differences in Z greater than 50 dBZ, Mann–Whitney U tests performed for Z greater than 0.5 dBZ show that the mean Z are statistically the same at a 95% confidence level. Comparisons of Z for simulations with different V_g (not shown) also showed statistically similar means. However, the

Mann–Whitney U tests show Z for the varying microphysics schemes have different means at higher altitudes in a statistically significant sense. Much of the difference in Z between microphysics schemes is related to the mixtures of phases and hydrometeor densities and choice of $N_{0(r,s,g)}$ used by the schemes to calculate Z in Eq. (1); differences between Z closer to the surface where all hydrometeors are rain are not as great. For example, the mean Z for points with $Z > 0.5$

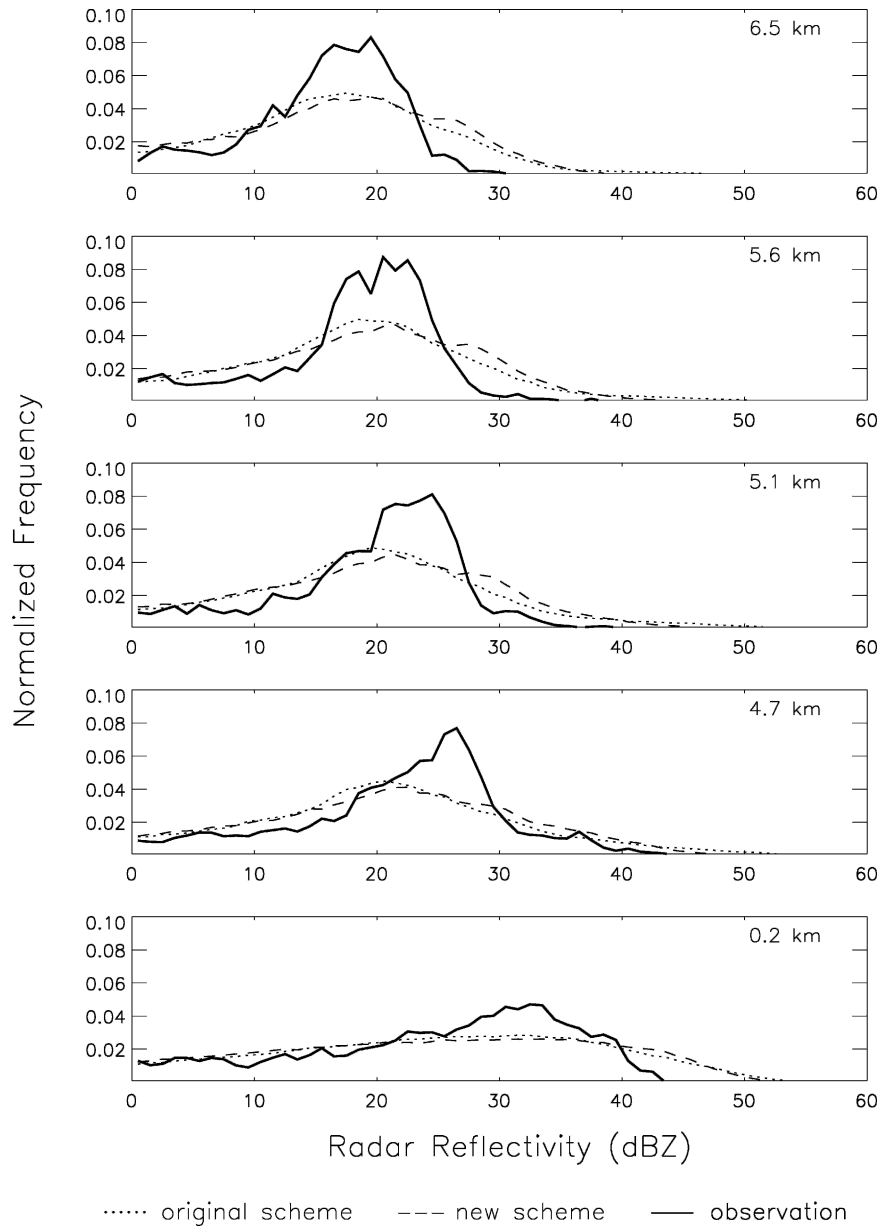


FIG. 12. As in Fig. 11 except lines depict modeled fields for base simulation and simulation with use of new iterative condensation scheme as indicated in the legend.

dBZ is 25.5 dBZ for the simple ice and Goddard schemes and 26.1 dBZ for the Reisner mixed-phase scheme. Thus, even though the improved condensation scheme (Fig. 9) and the choice of microphysics scheme have impacts on P_{\min} for Erin (Figs. 5 and 6), differences between simulations are not able to account for the systematic overestimates of large Z by the model.

Conversions between Z and R are dependent on assumptions made about the size distributions and compositions of the hydrometeors. For example, 45 dBZ can correspond to R of 20 or 35 mm h⁻¹ depending on

the Z - R relation. Thus, if simulations overestimate the frequency of Z above 35 dBZ at the surface, this does not necessarily indicate the frequency of the highest R is overestimated. Direct comparison with surface observations of R is not possible given that Erin did not achieve landfall. Nevertheless, it is informative to compare frequency distributions of rainfall between schemes to assess the sensitivity of modeled precipitation to representations of physics.

The total volume of rain reaching the ground averaged over the last 18 h of the simulation varies from

7.8×10^8 to 9.3×10^8 to $8.0 \times 10^8 \text{ m}^3 \text{ h}^{-1}$ for the simple ice, mixed-phase, and Goddard microphysics schemes, respectively. For each of these schemes, the instantaneous storm-total rainfall reaching the ground as a function of time varied by 29%, 36%, and 23% over the last 18 h from the average amount. This is similar to the behavior seen by Marks (1985), who found that the total water amount from Hurricane Allen stayed within about 40% since when Allen got stronger and peak R increased, the eyewall radius shrunk proportionally. Burpee and Black (1989) showed similar behavior in Hurricanes Alicia and Elena.

The mean R averaged over the last 18 h vary from 4.3 to 4.9 to 4.8 mm h^{-1} for simple ice, mixed-phase, and Goddard microphysics, respectively, and the standard deviations range from 10.0 to 11.8 to 11.5 mm h^{-1} for the same cases. Figure 13 shows how the area of the hurricane with R above the threshold plotted on the horizontal axis varies against R . The analysis again represents an average of the 18-h period from 0600 UTC 10 September to 0000 UTC 11 September with different line types representing varying microphysical schemes. The total area of the hurricane with R above 10 mm h^{-1} is on the order of $2 \times 10^4 \text{ km}^2$ and is within 5% for all three simulations. Here, R above 50 mm h^{-1} contributes about 15% to Erin's rain area for the Reisner mixed-phase and Goddard schemes, but only 11%–13% for the simple ice scheme. Differences between schemes are greater for R above 100 mm h^{-1} with the Goddard scheme producing more than double the area of the simple ice scheme, but these areas represent less than 0.2% of Erin's rain area. Compared to Frank (1977), who used rain gauges to show that the most intense rain occurring in the inner hurricane core had only 3% of its area with R greater than 23 mm h^{-1} and 16% greater than 7.5 mm h^{-1} , all simulations overestimate the frequency of heavy R . Although Frank's (1977) observations come from storms other than Erin and may be biased to low R by the hourly averages of the surface station data, this finding is consistent with the overestimate of Z in Fig. 11.

The presence of graupel above heavy rain regions in modeled fields indicates that melting graupel is a major source of rain (figure not shown). Given the same horizontal advection speed, graupel can advect further from the updrafts producing it for slower V_g , spreading it over larger areas, which would give less intense rain for slower V_g and more intense rain for faster V_g given the same total water. For simulations evidence of such behavior is noted as areas with $R > 50 \text{ mm h}^{-1}$ contribute 15% to the total rain area for fast V_g and only 10% for slow V_g ; differences in hurricane area with $R > 10 \text{ mm h}^{-1}$ are negligible or less than 5% (figure not shown).

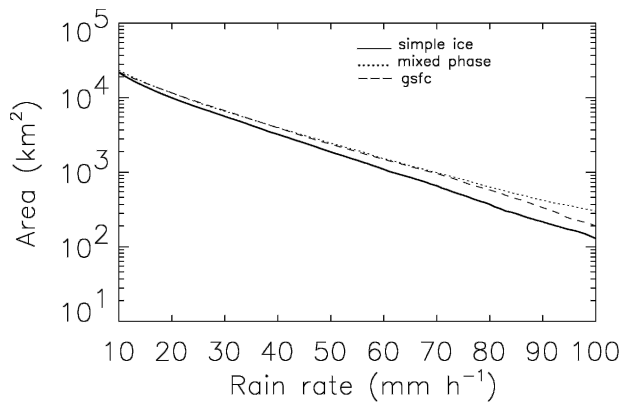


FIG. 13. Area (km^2) of simulated hurricane, having R above threshold plotted on the horizontal axis at 0000 UTC 11 Sep 2001. Different line types represent different microphysical parameterization schemes as indicated in the legend. Averages of last 18 h of modeled fields are used to construct plot.

Dynamical effects associated with varying distributions of latent heating and cooling produced by hydrometeor conversions in different simulations complicate relationships between P_{\min} , V_g , and rain distributions.

Similar analysis of surface R is conducted for the other sensitivity studies. Figure 14 shows the variation of hurricane area with R above a threshold for varying boundary layer schemes. Different behavior than that depicted in Fig. 13 is noted in that the total area of the storm with $R > 10 \text{ mm h}^{-1}$ varies by up to $9 \times 10^3 \text{ km}^2$ between simulations. The Eta scheme that gives the lowest P_{\min} and highest U_{\max} has the greatest surface rain area of $2.7 \times 10^4 \text{ km}^2$ and the Blackadar scheme that gives the least intense hurricane has the lowest surface rain area of $1.8 \times 10^4 \text{ km}^2$. For all boundary layer schemes over 10% of the simulated hurricane rain area has R greater than 50 mm h^{-1} , again showing more

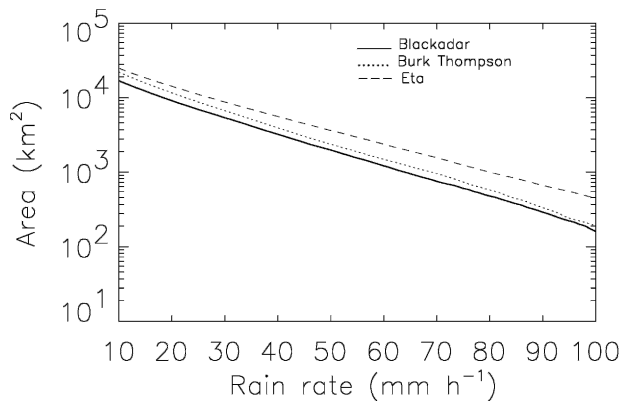


FIG. 14. As in Fig. 13, except different line types correspond to simulations using different boundary layer schemes as indicated in legend.

frequent heavy rain rates than seen in the Frank (1977) observations. Differences between boundary layer schemes alone are again not able to explain systematic offsets between R distributions from observations and simulations of Erin.

Figure 15 compares Erin's area above a threshold R for a base simulation using Reisner mixed-phase microphysics and a simulation using an iterative condensation scheme. Erin's area with R above 10 mm h^{-1} is almost identical for the two simulations. However, Erin's area with R above about 50 mm h^{-1} is more sensitive to the choice of condensation scheme than to choice of microphysical scheme (Fig. 13), boundary scheme (Fig. 14), or V_g . For example, for R greater than 50 (100) mm h^{-1} , the iterative scheme gives an area for Erin one-half (one-tenth) that of the base scheme. The reduced occurrence of high R for the iterative scheme is logical because high R typically occurs within the intense rainband at the hurricane eyewall where conventional schemes would most overpredict condensation and rain. Although the area where the iterative condensation scheme reduces R represents less than 10% of Erin's rain area, impacts on dynamics are noteworthy given differences in P_{\min} and U_{\max} .

To further investigate the role of graupel in overpredicting large R and Z , normalized frequency distributions of graupel mixing ratio q_g are plotted in Fig. 16 for the control simulation with Goddard microphysics and varying V_g . Regardless of V_g , simulated q_g are higher by an order of magnitude than observations in Hurricane Norbert 1984 and Hurricane Emily 1987 where graupel mass contents seldom exceeded 0.1 g m^{-3} (Fig. 12 of McFarquhar and Black 2004), corresponding to q_g of approximately 0.2 g kg^{-1} at a pressure of 500 hPa. Although not obtained in Erin, the data represent the two different conditions that can be encountered in hurricanes: observations in Norbert were obtained in stratiform areas outside the eyewall (Black 1990), whereas observations in Emily were made in unusually strong updrafts and downdrafts in the eyewall during its deepening phase (Black et al. 1994). Mann-Whitney U tests showed no significant difference in mean q_g for the simulations with different V_g , showing that even though graupel fall speed impacts P_{\min} and U_{\max} , it cannot correct for the likely overestimate of q_g .

To further evaluate the simulated hydrometeor mixing ratios, T_b computed from simulations are compared against T_b observed by AMPR; T_b was computed using a radiative transfer model (C. Kummerow 2004, personal communication) that calculated scattering and emission from the different hydrometeor species. The densities and exponential intercept parameters were separately set for each hydrometeor category to match

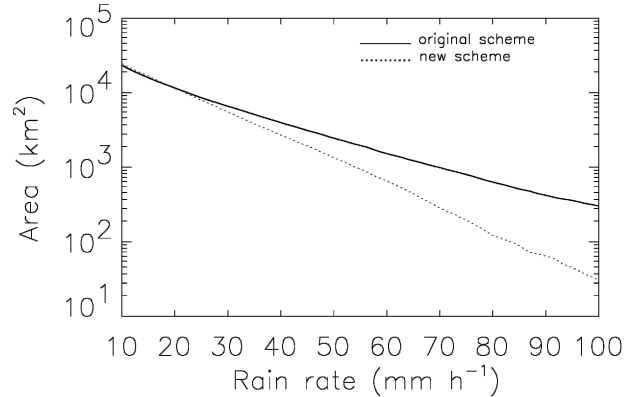


FIG. 15. As in Fig. 13, except different line types correspond to base simulation and simulation with use of new iterative condensation scheme.

the model assumptions used in MM5. Figure 17 compares observed and predicted normalized frequency of T_b in the four AMPR channels where the simulated T_b distributions are obtained using modeled fields from 1800 UTC on 10 September and the observed T_b are obtained using data from all ER-2 sorties. Regions corresponding to the eye have been removed from both models and observations so that different eye sizes do not dominate a comparison of the frequency distributions. For the 10.7- and 19.35-GHz channels dominated by thermal emission from rain, simulations overestimate the frequency of T_b greater than 235 K, but underestimate that between 150 and 235 K. Since larger T_b corresponds to higher R and Z , this is consistent with trends noted in Figs. 10–12.

At 37.1 GHz, the model underestimates the frequency of T_b between 255 and 280 K, but overestimates that between 190 and 255 K. Mann-Whitney U tests show the differences are statistically significant. The 37.1-GHz channel responds to the emission of rain with the presence of graupel reducing the emission signal through scattering. For T_b calculated from modeled hydrometeor fields with q_g set to zero (and all other hydrometeor fields the same as in the control simulation), the less frequent occurrence of T_b values between 200 and 260 K, consistent with observations, suggests an overprediction of graupel is responsible for at least part of the discrepancy with observations. Between 255 and 280 K T_b is underpredicted in the control simulation because the scattering that reduces the emission at 37.1 GHz results in fewer large T_b in a normalized frequency distribution. The overprediction of T_b between 190 and 220 K compared to observations corresponds to regions without rain or graupel. At 85.5 GHz there is a long narrow tail for T_b between 140 and 230 K in the simulation that is not present when the contributions due to

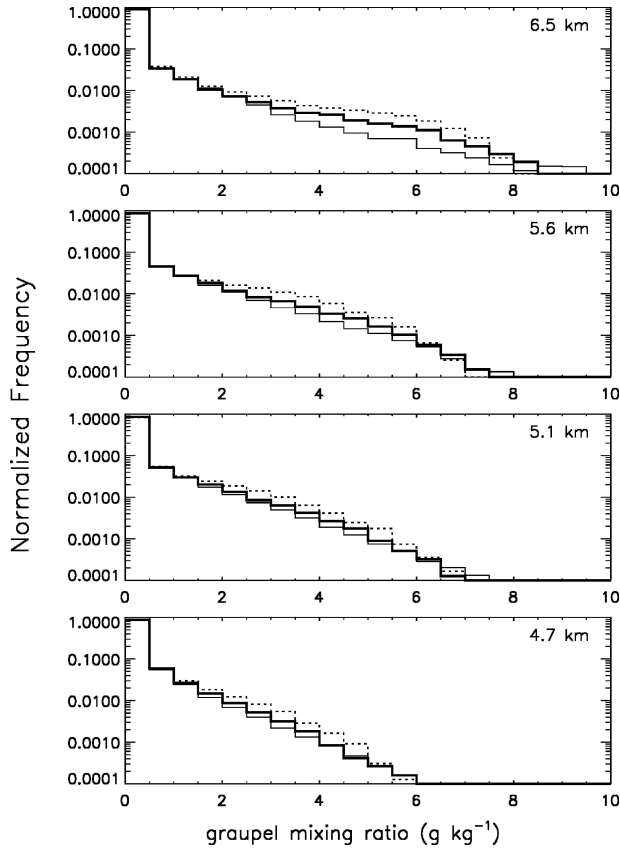


FIG. 16. Histograms of graupel mixing ratio q_g for simulations with varying V_g : thick solid lines represent base V_g , dotted lines represent slower V_g , and thin solid lines represent faster V_g . Histograms computed from modeled fields corresponding to last 18 h of simulations.

q_g are excluded in the radiative transfer calculations. Because this tail is also not present in the observations, this suggests that a significant amount of graupel is not present during the three overpasses. There is also an offset between the observed frequency peak at 260 K and the simulated peak at 270 K.

To identify potential causes of graupel overprediction, the relationship between its spatial distribution and the convection producing it is examined. Figure 18 shows q_g and updraft velocity as a function of distance from the hurricane center for simulations with varying V_g . Different angles of cross section are selected for each panel in Fig. 18 to ensure that an intense rainband and graupel are included. Graupel occurs over a narrow band of 10–40 km, well correlated with the location of the updraft regardless of the V_g scheme. Scatterplots of q_g and updraft velocity further showed that when updrafts were stronger than 2–3 m s^{-1} , q_g was typically larger than about 2 g kg^{-1} . There are no in situ penetrations for Erin that would be required to do an

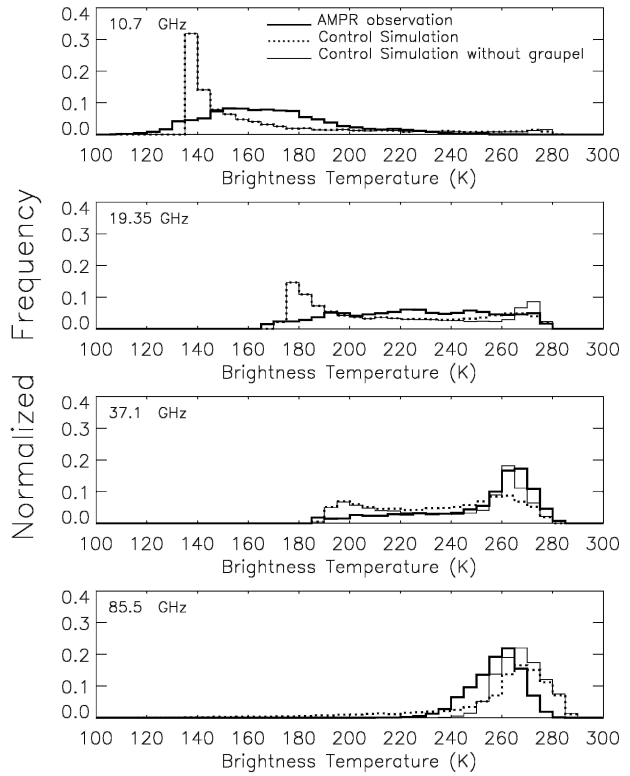


FIG. 17. Histograms of brightness temperature T_b observed and computed using modeled fields at the four operating frequencies of AMPR. Points corresponding to modeled and observed eye location have been removed from T_b sample; T_b from modeled fields corresponding to 1800 UTC 10 Sep used to construct histograms.

equivalent correlation analysis for observations. However, this does show that the vertical motion characteristics must be examined to understand sources of graupel.

d. Impacts on vertical motion

The above analysis suggests that simulations overpredict the frequency of heavy rain and large Z for Erin regardless of which representations are used. However, large differences in P_{\min} and U_{\max} between simulations still occur most likely because varying distributions of latent heating and cooling feed back on dynamics and affect the structure and evolution of Erin. To investigate how physical processes affect vertical motion, statistical distributions of updrafts and downdrafts are examined. An updraft or downdraft is defined here as any grid box where the vertical air velocity w is greater than 1 m s^{-1} or less than -1 m s^{-1} . This is similar to definitions used by Jorgensen et al. (1985) and Houze (1993) in that Jorgensen’s definition assumed that these air

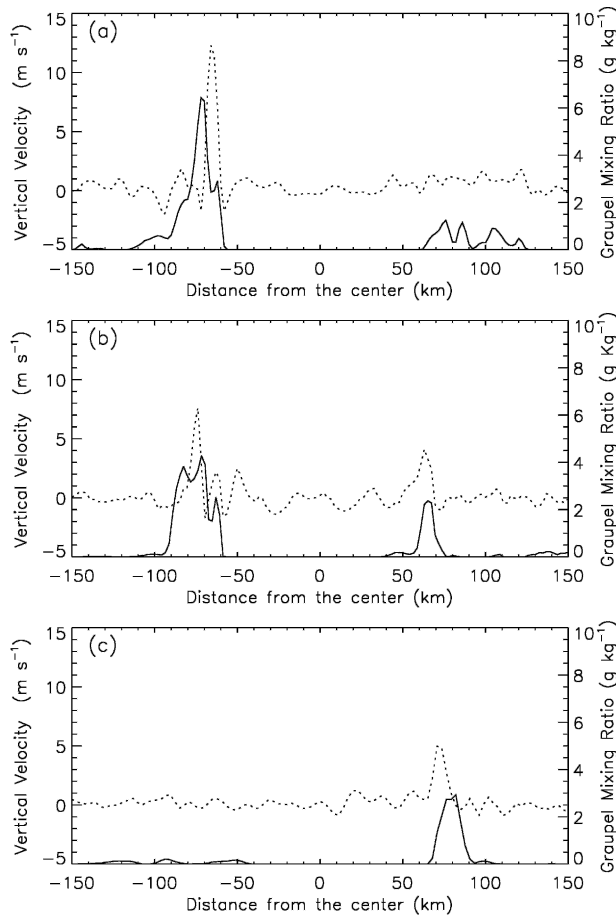


FIG. 18. Plot of graupel mixing ratio (solid line) and vertical velocity (dashed line) at temperature of -5°C for varying distance along a cross section that cuts through the eye of the hurricane. Plots from top down represent base simulation with original V_g , simulation with slow V_g , and simulation with fast V_g .

speeds existed in aircraft observations for 5 consecutive seconds, which corresponds to about 1 km, and Houze's definition assumed the air motion had a greater magnitude than the fall velocities of stratiform ice particles, which is on the order of 1 m s^{-1} .

For the same altitudes near the freezing level shown in Fig. 11, Fig. 19 shows normalized frequency distributions of updrafts and downdrafts for different microphysical schemes. Only grid boxes with vertical motion greater than or less than 1 m s^{-1} are included. Except for the strongest updrafts above 5 m s^{-1} representing less than 5% of updrafts, distributions from simulations with varying microphysics do not show large differences. Mann-Whitney U tests confirmed that there are no significant differences at a 0.05 confidence level even when the strongest updrafts are included in the distributions. Similar tests showed that differences in downdraft distributions are not significant. For simula-

tions with varying V_g (figure not shown), updraft and downdraft distributions again exhibited no significant differences at a 0.05 confidence level.

There are no direct observations of updrafts and downdrafts covering multiple altitudes from Erin. However, a comparison against vertical velocity statistics analyzed from seven Atlantic hurricanes (Black et al. 1996) is made. Figure 21 shows the updraft (downdraft) magnitude below which 70% and 95% of the modeled updrafts (downdrafts) occur as a function of altitude for the control simulation using Goddard microphysics. The panels show statistics for four separate regions: eyewall, rainbands, stratiform, and the entire hurricane. For simulations, the eyewall represents locations within 80 km of the eye where $Z > 30 \text{ dBZ}$. Regions outside the eyewall are defined as rainbands if $Z > 30 \text{ dBZ}$ or as stratiform if $10 < Z < 30 \text{ dBZ}$. Black et al. (1996) defined regions similarly, with the eyewall being regions with quasi-annular maxima in horizontal Z patterns and elongated Z maxima in the vertical, rainbands regions with $Z > 30 \text{ dBZ}$ outside the eyewall and the stratiform region as horizontally homogeneous regions with $10 < Z < 30 \text{ dBZ}$.

Exact agreement between Fig. 21 and the Black et al. (1996) statistics would not be expected even if the model perfectly represented processes occurring in hurricanes because the observations were not obtained in Hurricane Erin and because of inevitable uncertainties in the techniques Black et al. (1996) used to calculate air motion by removing Z -dependent particle fall speeds (Marks and Houze 1987). Nevertheless, trends can be compared. Figure 5 of Black et al. (1996) show 70% of w within $\pm 2 \text{ m s}^{-1}$ in each region. With the exception of updrafts at heights above 5 km where 30% of w are greater than 3 m s^{-1} at 6 km and greater than 6 m s^{-1} at 10 km in the eyewall, the same is true for the simulations. Just as Black et al. (1996) noted the broadest distributions of vertical motion in the eyewall where 5% of updrafts exceeded 5 m s^{-1} and 5% of downdrafts exceeded 3 m s^{-1} , the control simulation shows the broadest distribution of vertical motion in the eyewall with 5% of w stronger than 5 m s^{-1} at 4-km altitude and 5% stronger than 10 m s^{-1} at 9 km. The simulated updrafts at higher altitudes are larger than the values found by Black et al. (1996) in the eyewall, who observed that w increased with height but not as quickly as in the simulations. The weakest values and narrowest distributions of vertical motion are found in the stratiform regions for both simulations and observations, with 5% of w less than $\pm 2 \text{ m s}^{-1}$ except for simulated w at altitudes above 11 km that have larger values. For the model, the rainbands represent an intermediate region between the eyewall and stratiform area as in observa-

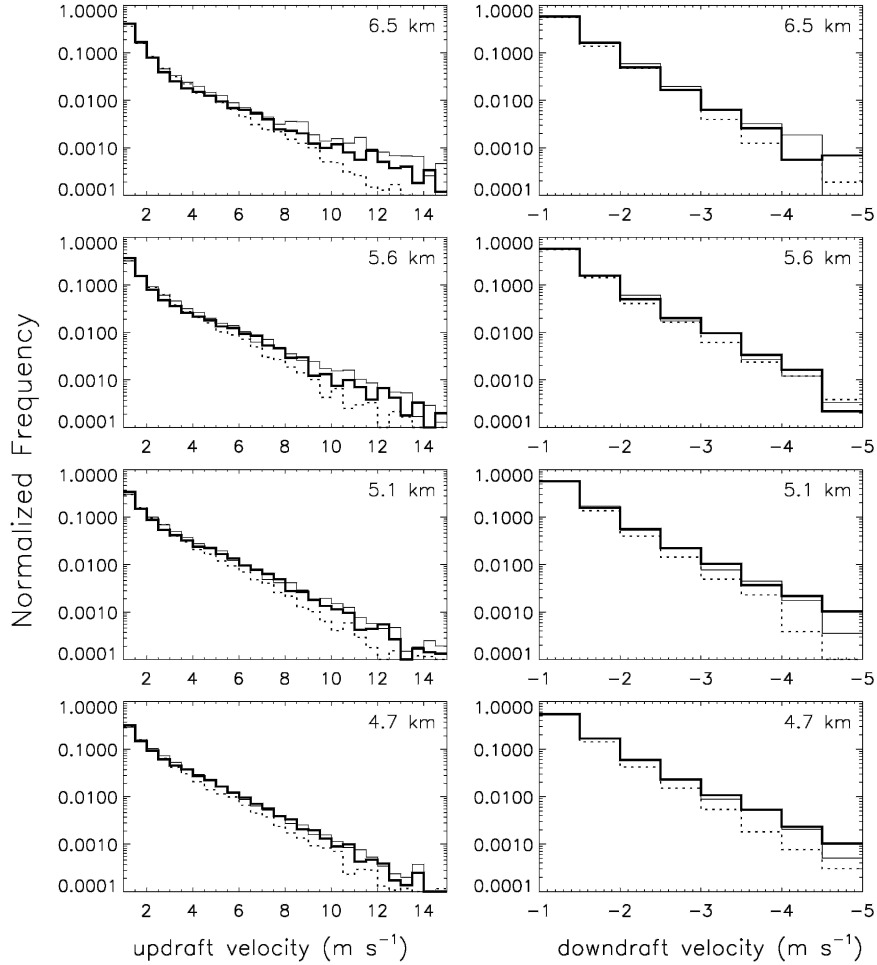


FIG. 19. Histograms of frequency of occurrence of vertical updrafts and downdrafts having magnitude above 1 m s^{-1} for simulations with varying microphysical parameterization schemes: light solid, simple ice scheme, dashed, Reisner mixed-phase scheme, dark solid, Goddard scheme. Different panels represent distributions at different σ levels, corresponding to the labeled heights and temperatures of approximately -11° , -4° , -1° , and 0°C . Histograms computed from modeled fields corresponding to last 18 h of simulation.

tions; 5% of observed updrafts (downdrafts) are less than 5 (3) m s^{-1} , as also seen in simulations except for stronger updrafts that occur at altitudes between 6 and 9 km in the models. These comparisons are thus consistent with models overestimating vertical motion at altitudes between 6 and 10 km.

Computing V_{dop} from modeled fields and comparing against EDOP allows an indirect comparison of modeled and observed w if it is assumed the model adequately represents particle fallout. This is a more direct comparison than using the Black et al. (1996) statistics because all uncertainties about particle fall velocities are isolated in the modeled fields and because the observations come from Hurricane Erin. At the very least, alternate fall speed assumptions are not used in retrievals and models. Figure 22 compares V_{dop} sta-

tistics from EDOP against those calculated from modeled fields for the same four altitudes near the melting layer shown in Fig. 11 for the Goddard microphysics scheme with varying V_g . The V_{dop} is calculated by adding w to the Z -weighted fall speeds of modeled particle distributions. Negative V_{dop} represents motion toward the aircraft. The frequency of occurrence of V_{dop} between -2 and -18 m s^{-1} at an altitude of 6.5 km, corresponding to about -11°C , is overpredicted compared to observations. This is consistent with the suggested overprediction of strong updrafts at this level (Fig. 21) compared to the Black et al. (1996) statistics. A similar overprediction of negative V_{dop} is seen at higher levels (figure not shown) and occurs regardless of the V_g or microphysical parameterization used. However, some caution must be exercised in this comparison because

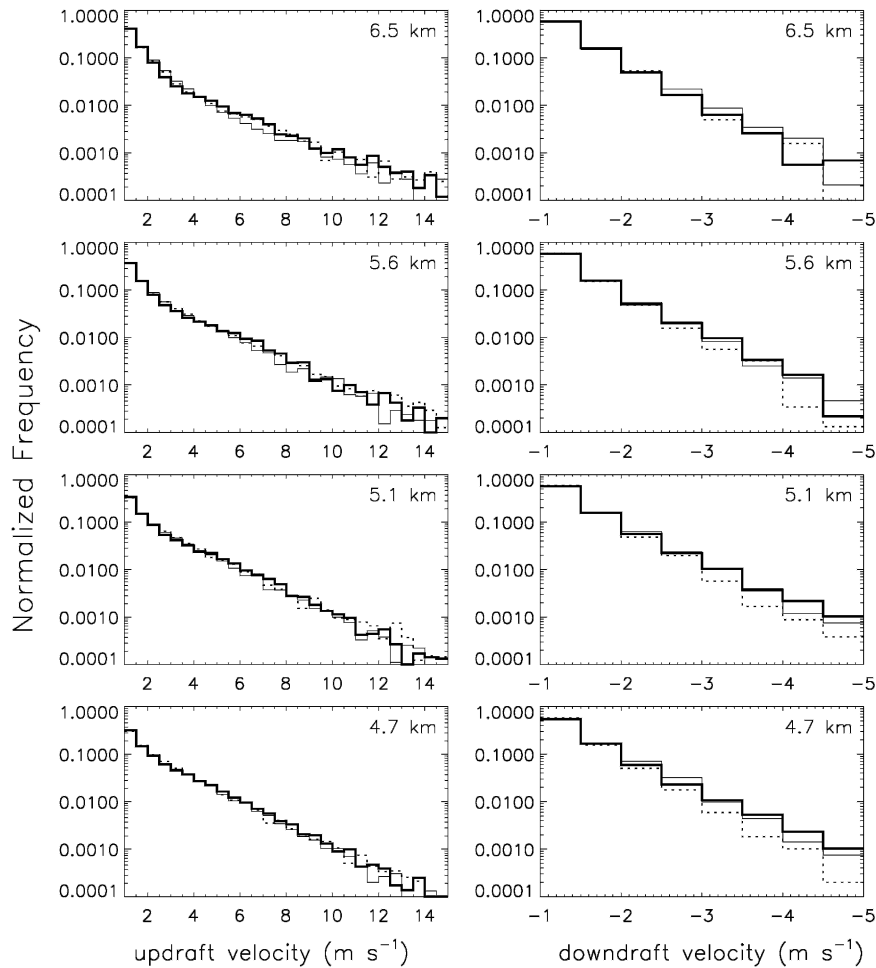


FIG. 20. As in Fig. 19, except for simulations with varying representations of graupel fall speed: dark solid, original simulation; dotted, slower V_g ; light solid, faster V_g .

the EDOP observations were collected when U_{\max} was decreasing and Erin starting to decay.

For the three layers closest to the freezing level in Fig. 22 it cannot be categorically stated that modeled V_{dop} between -5 and -10 m s^{-1} is overestimated because of sampling issues. For the 5.6-, 5.1-, and 4.7-km levels, points with V_{dop} between -1 to -5 m s^{-1} represent 99% of the data. If V_{dop} less than -5 m s^{-1} existed in the real Erin, they might not be observed by EDOP as the ER-2 made only three sorties through the storm sampling a small fraction of the hurricane. For these three levels, it appears that closer to the freezing level the model starts to underestimate the normalized frequency of V_{dop} between -2 and -5 m s^{-1} . Mann-Whitney U tests show differences between models and observations are statistically significant. The impact of this difference is important because approximately 20% of upward V_{dop} between -2 and -5 m s^{-1} occur at these levels. Thus, comparison against observed V_{dop}

suggests that either assumed fall velocities in the model are incorrect near the melting level or that modeled updrafts may be underpredicted there. Alternatively, since vertical velocity gradients are largest near the melting layer and since the melting layer altitude varies by up to 0.7 km excluding the eye in the Erin simulations, temperature differences at given altitudes may account for some of the discrepancies between observed and simulated V_{dop} . The suggested overprediction for the 6.5-km level and above is different. For downdrafts, for the 4.7- and 5.1-km levels closest to the melting layer positive values of V_{dop} between 2 and 5 m s^{-1} occur more frequently in observations than in models, whereas V_{dop} values between 5 and 15 m s^{-1} occur more frequently in models. For the two higher levels (5.6 and 6.5 km), the model underpredicts the frequency of occurrence of V_{dop} values greater than 3 m s^{-1} . These differences might be attributed to production of smaller downdrafts by the model; a representa-

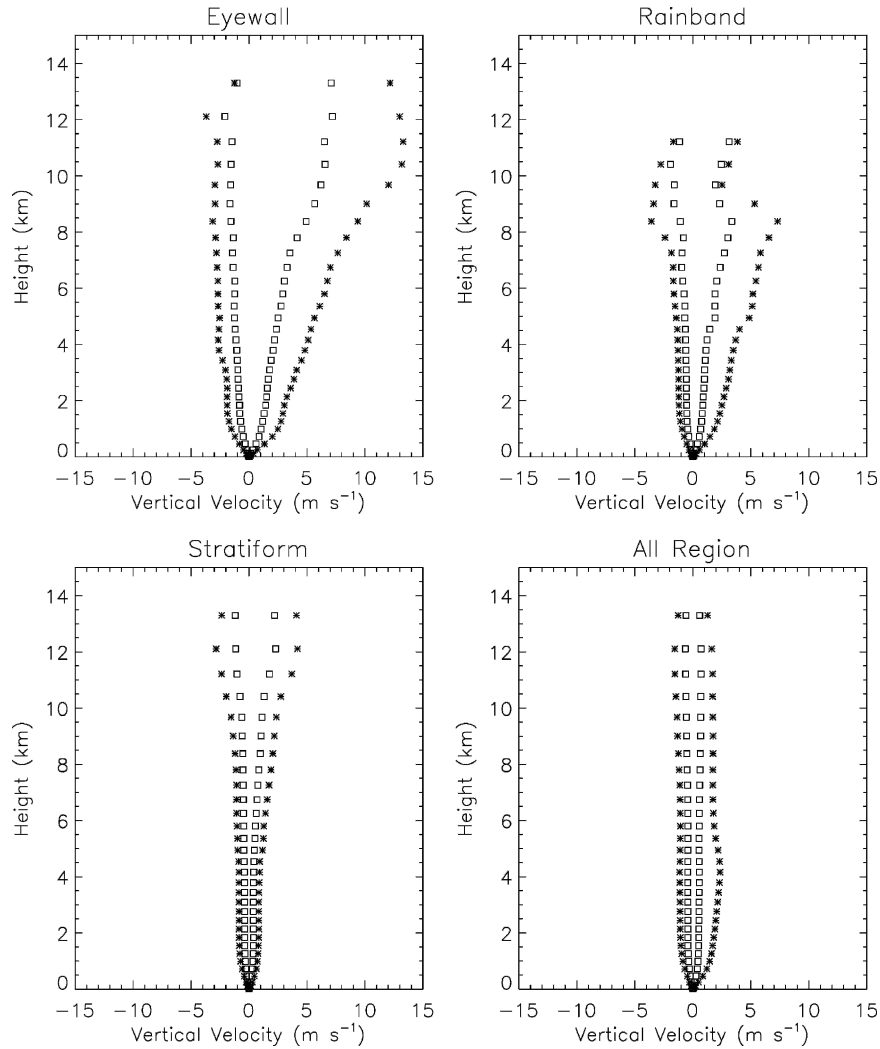


FIG. 21. Frequency distributions of vertical motion in four different regions of Hurricane Erin, constructed from modeled fields corresponding to last 18 h of simulation. Squares represent vertical motion for given height below which 70% of upward (downward) motion is below (above); asterisks correspond to vertical motion for which 95% of values are above or below.

tion of particle fall speed that does not match the observations may also contribute to these differences.

Figures 19, 20, and 22 show that differences in V_{dop} and in updraft/downdraft statistics between simulations with varying representations of microphysics or V_g are smaller than the differences between simulations and observations. Figure 23 shows the representation of condensation can impact updraft statistics as, for example, the frequency of updrafts larger than 5 m s^{-1} is reduced from 2% to 0.06% at a height of 5.1 km; similar differences are seen at other altitudes including those altitudes not shown in Fig. 23. Mann–Whitney U tests show that the use of the iterative condensation scheme does not impact the mean downdraft.

Lower values of the largest R and Z and strongest w were also produced with the iterative condensation scheme, but contributed minimally to hurricane rain area. The use of the iterative condensation scheme also cannot explain systematic offsets in these fields from observations. Although overestimates of moisture associated with some condensation schemes may not have detectable effects on the Z distributions, the artificial increase in latent heating may have big impacts on hurricane dynamics and feedbacks on hurricane intensity and evolution as Fig. 9 previously showed the new condensation scheme could give P_{min} up to 12 hPa higher and U_{max} up to 6 m s^{-1} lower for the simulations of Erin compared to conventional schemes.

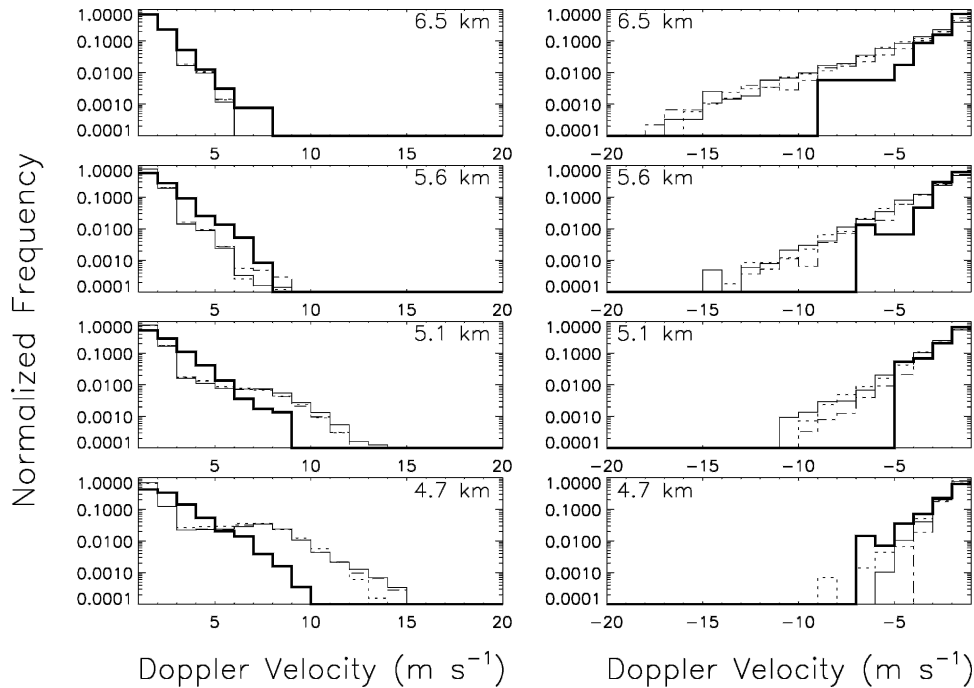


FIG. 22. Observed and simulated V_{dop} for four different altitudes. Negative V_{dop} represents upward motion toward aircraft. Dark solid line corresponds to observations; thin line, base simulation; dashed line, slower V_g simulations; and dash-dot, faster V_g simulations.

e. Impacts on inner eye thermodynamics

Figure 24 compares vertical profiles of T and T_d produced using the iterative condensation scheme against those produced from the base simulation and measured in Erin's eye. Below 2 km, T and T_d profiles simulated by the iterative condensation are more consistent with those observed than predicted by conventional schemes. However, with the iterative scheme, the substantial dry layer observed and obtained in the base simulation between 2 and 10 km, while present, is not as dry. For example, the dewpoint depression at 5 km is 16°C for both the base simulation and observations but only 6°C for the iterative scheme. Because the new scheme leads to less condensation in the eyewall, the enhanced q_v in the modeled eye would be consistent with this extra, uncondensed vapor mixing with dry air in the eye. Alternatively, the moister eye is also consistent with the weaker updrafts produced by the new condensation scheme being less efficient at transporting water vapor to higher levels and away from the eye allowing more moisture to reach the eye. Yet another possibility is that less convection could lead to less subsidence in the eye hindering the development of the dry layer.

It is also noted that the lower Θ_e near the surface calculated from the simulation using the iterative con-

densation scheme is more consistent with Θ_e calculated from the dropsonde profile compared to those calculated with the conventional condensation scheme. A more thorough investigation of how condensation affects the development of the dry layer within the eye is beyond the scope of this paper.

5. Conclusions

Simulations of Hurricane Erin 2001 were conducted with MM5 to examine roles of microphysical, thermodynamic, and boundary layer processes on hydrometeor distributions and on the structure and evolution of Erin. Statistical comparisons of modeled fields with observations collected during CAMEX-4 and in other hurricanes are used to assess the importance of physical processes acting within Erin. Because of the complexity of interactions between different processes, it is impossible to categorically state the sensitivity to any single process or parameterization scheme. Nevertheless the following conclusions can be made:

- 1) The representation of boundary layer processes is crucial in determining the strength of the simulated Erin with U_{max} and P_{min} averaged over the last 18 h varying by over 10 m s^{-1} and 20 hPa depending on the scheme. Consistent with past studies, the Burk-

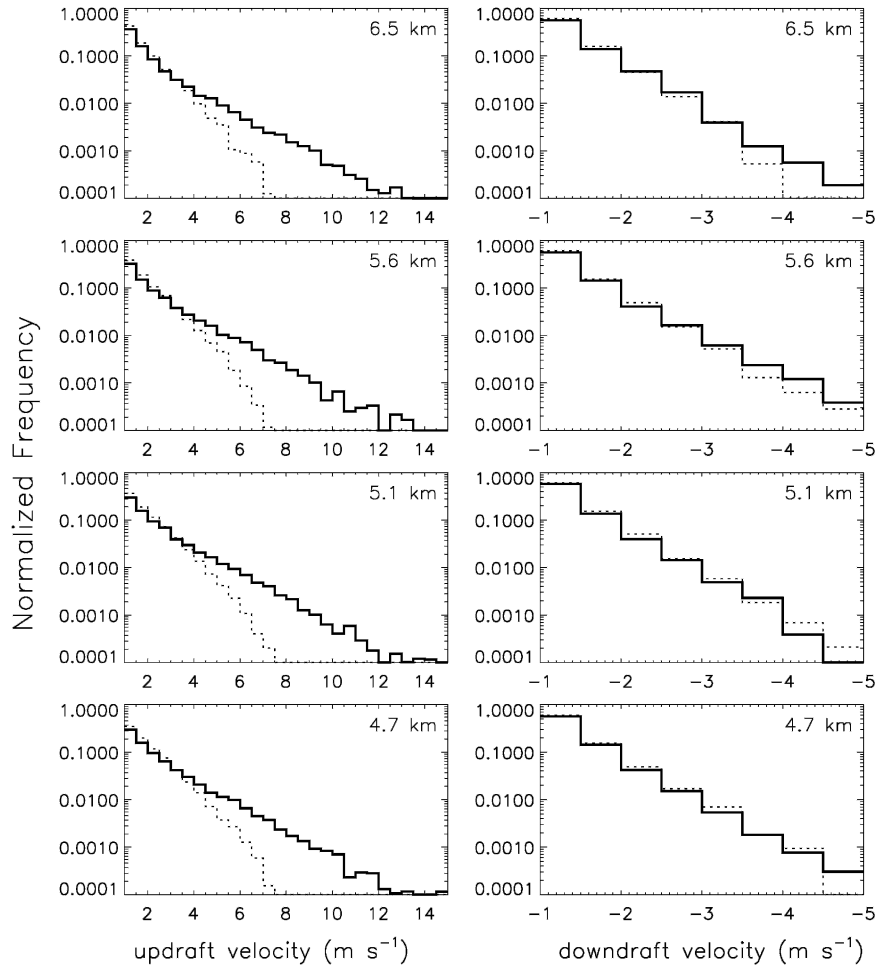


FIG. 23. As in Fig. 19, except solid line represents base parameterization scheme and dashed line represents simulations with new iterative condensation scheme.

Thompson (1989) and Eta boundary layer schemes give a more intense hurricane.

- 2) The choice of microphysical parameterization scheme and of coefficients to describe graupel fall velocities have similar impacts on the simulated intensity of Erin, with U_{\max} and P_{\min} varying by up to 7 m s^{-1} and 9 hPa for different schemes and by 5 m s^{-1} and 7 hPa for different V_g . In general, schemes with more detailed physics and faster V_g give lower P_{\min} and higher U_{\max} .
- 3) Variations between microphysics, boundary layer, convection or V_g schemes are not large enough to explain discrepancies between modeled and observed Z and q_g , as consistent overprediction of Z greater than 40 dBZ near the surface, of Z greater than 25 to 30 dBZ near the melting level and of q_g was found.
- 4) The use of an iterative condensation scheme developed to limit the artificial increase of Θ_e associated

with some condensation schemes reduced simulated U_{\max} and P_{\min} by 5 m s^{-1} and 7 hPa , respectively. Its use reduced the occurrence of updrafts stronger than 5 m s^{-1} and of Z above 50 dBZ , but did not significantly impact the overprediction of Z between 35 and 50 dBZ . Given the scheme's big impact on hurricane intensity, the effect of latent heating occurring within a few strong updrafts on Erin's evolution is seen.

- 5) Comparison of T_b observed against that simulated from modeled fields shows models overpredict contributions from scattering at the 37.1 - and 85.5 -GHz channels, consistent with the model overpredicting graupel or underpredicting supercooled water; comparison of q_g against in situ observations of graupel in other hurricanes suggests that it may be the former.
- 6) Compared to V_{dop} measured by EDOP and updraft and downdraft statistics observed in other hurri-

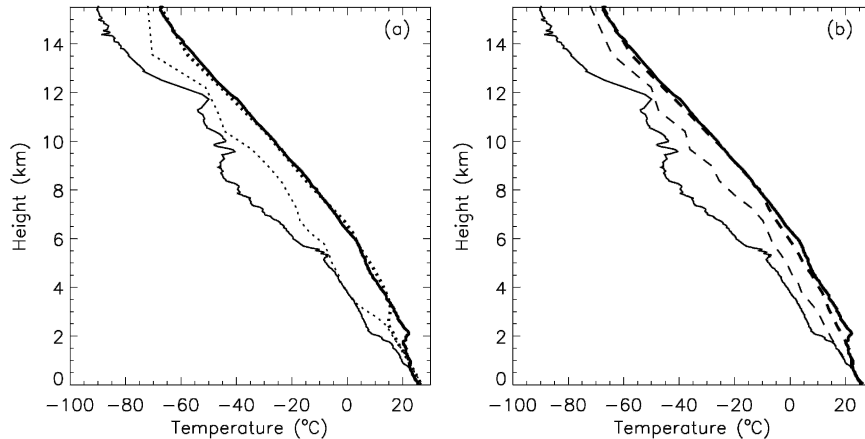


FIG. 24. Vertical profile of temperature and dewpoint temperature from dropsonde observations (solid line) and for model simulations (dotted and dashed lines): (a) simulation with base condition and (b) simulation with new iterative condensation scheme.

canes, the frequency of updrafts stronger than 2 m s^{-1} is overpredicted by the Erin simulations for altitudes higher than 6 km.

Our finding of stronger simulated vertical motions than observed (Black et al. 1996) differs from Rogers et al.'s (2004) findings of weaker simulated vertical motions. Furthermore, Rogers et al. found that their simulated motions narrowed with height, trends not noted for the altitude levels examined here. Further investigations on these discrepancies, together with their dependence on model horizontal and vertical resolution, are required. Dependence on kinematic structures that ultimately control microphysical processes must also be further assessed in these investigations.

Different hurricanes have widely varying amounts of condensate so caution must be exercised when extrapolating results pertaining to Erin to other hurricanes. Further, if one parameterization scheme that artificially weakens a hurricane is used with another parameterization that artificially strengthens it, the final result may look reasonable. Future studies must place more emphasis on physical processes occurring within hurricanes and on the development of parameterization schemes with more physical basis. Future model simulations with finer resolutions, bin-resolved or multimoment microphysical, and more resolved boundary layer processes should also help acquire a better understanding of hurricanes.

Acknowledgments. This research was sponsored by the NASA CAMEX-4 Grant CAMEX-0000-0024. The findings do not necessarily represent the views of NASA. The NOAA P-3 radar imagery was obtained from the Hurricane Research Division of NOAA. The

remaining data were obtained from the CAMEX-4 archive at the Global Hydrology Resource Center sponsored by the NASA Atmospheric Dynamics and Remote Sensing Program. Frank LaFontaine provided the AMPR images and Chris Kummerow provided the microwave radiative transfer code. The advice and assistance of Frank LaFontaine, Dan Cecil, Scott Braun, and three anonymous reviewers is acknowledged.

APPENDIX

Iterative Condensation Scheme

Bryan and Fritsch (2000) documented unphysically high values of Θ_c in their simulations of cumulonimbus clouds using MM5, noting that these problems existed regardless of the microphysics or boundary layer scheme. A major reason for the high values of Θ_c calculated was that the one-step condensation equation used tended to overestimate the final value of mixing ratio and temperature, especially in the presence of vigorous updrafts. It is unknown what effects this problem may have had on past hurricane simulations, but it may be partially responsible for the higher simulated precipitation rates than found in observations. A new iterative condensation scheme is derived here to more accurately predict the modeled condensation rate.

In version 3.5 of MM5, temperature and vapor pressure are stepped forward at each time without condensation occurring, then an adjustment step is made converting excess vapor to liquid water so that the air is saturated. Following Grell et al. (1995), (q_i, T_i) represent the temperature and vapor pressure before the adjustment step. If q_i is greater than $q_{s,i}$, the saturated vapor pressure at T_i , condensation will occur so that $(q_f,$

T_f) represent the vapor pressure and temperature after condensation and represent saturated conditions, with $q_f < q_i$ and $T_f > T_i$. The points (q_{si}, T_i) and (q_f, T_f) are connected by the Clausis–Clapeyron equation, given by

$$\frac{dq_s}{dT} = \frac{q_f - q_{si}}{T_f - T_i} = \frac{q_s L_v}{R_v T^2}, \quad (\text{A1})$$

where R_v is the gas constant and L_v the latent heat of vaporization. The slope of the line between points (q_i, T_i) and (q_f, T_f) is determined from moist static energy conservation,

$$L_v dq = L_v(q_f - q_i) = -c_p dT = -c_p(T_f - T_i). \quad (\text{A2})$$

In the scheme implemented in MM5, the temperature in Eq. (A1) is assumed to be T_i , and can lead to a substantial overestimate of the amount of condensation occurring within a time step. For example, assuming an increase of 0.1°C at a temperature of 20°C , the condensation rate would be overestimated by 0.25% by Eq. (A2). Although this may not seem significant, when integrated over an entire hurricane simulation, this systematic error might be problematic. Further, given that air masses may rise a couple hundred meters in a given time step, the 0.1°C increase per time step is likely an underestimate.

Although it may be advantageous to develop a condensation scheme that uses Θ_e as an advective variable, the problem of overestimating condensation can be simply corrected through the development of an iterative condensation scheme. The temperature used in Eq. (A1) is assumed to be the average of T_f and T_i to make a more accurate estimate of condensation, the final temperature, and water vapor content. This is an iterative calculation because q_f and T_f must be recomputed a few times until the solution converges. Because the solution rapidly converges, minimal extra computational expense is required.

REFERENCES

- Aberson, S., J. Dunion, and F. D. Marks Jr., 2006: A photograph of a wavenumber-2 asymmetry in the eye of Hurricane Erin. *J. Atmos. Sci.*, **63**, 387–391.
- Black, M. L., R. W. Burpee, and F. D. Marks, 1996: Vertical motion characteristics of tropical cyclones determined with airborne Doppler radial velocities. *J. Atmos. Sci.*, **53**, 1887–1909.
- Black, R. A., 1990: Radar reflectivity–ice water content relationships for use above the melting layer in hurricanes. *J. Appl. Meteor.*, **29**, 955–961.
- , H. B. Bluestein, and M. L. Black, 1994: Unusually strong vertical motions in a Caribbean hurricane. *Mon. Wea. Rev.*, **122**, 2722–2739.
- Braun, S. A., and W.-K. Tao, 2000: Sensitivity of high-resolution simulations of Hurricane Bob (1991) to planetary boundary layer parameterizations. *Mon. Wea. Rev.*, **128**, 3941–3961.
- Bryan, G. H., and J. M. Fritsch, 2000: Unphysical thermodynamic structures in explicitly simulated thunderstorms. *10th Annual Penn State/NCAR MM5 User's Workshop*. [Available online at <http://www.mmm.ucar.edu/mm5/mm5-home.html>.]
- Burk, S. D., and W. T. Thompson, 1989: A vertically nested regional numerical prediction model with second-order closure physics. *Mon. Wea. Rev.*, **117**, 2305–2324.
- Burpee, R. W., and M. L. Black, 1989: Temporal and spatial variations of rainfall near the centers of two tropical cyclones. *Mon. Wea. Rev.*, **117**, 2204–2218.
- Cecil, D. J., and E. J. Zipser, 2002: Reflectivity, ice scattering, and lightning characteristics of hurricane eyewalls and rainbands. Part II: Intercomparison of observations. *Mon. Wea. Rev.*, **130**, 785–801.
- Doviak, R. J., and D. S. Zrnic, 1984: *Doppler Radar and Weather Observations*. Academic Press, 458 pp.
- Dudhia, J., 1989: Numerical study of convection observed during the winter monsoon experiment using a mesoscale two-dimensional model. *J. Atmos. Sci.*, **46**, 3077–3107.
- Frank, W. M., 1977: The structure and energetics of the tropical cyclone. Part I: Storm structure. *Mon. Wea. Rev.*, **105**, 1119–1135.
- Grell, G. A., J. Dudhia, and D. R. Stauffer, 1995: A description of the fifth-generation Penn State/NCAR Mesoscale Model (MM5). NCAR Tech. Note NCAR/TN-398+STR, 117 pp.
- Halverson, J. B., J. Simpson, G. Heymsfield, H. Pierce, T. Hock, and L. Ritchie, 2006: Warm core structure of Hurricane Erin diagnosed from high-altitude dropsondes during CAMEX-4. *J. Atmos. Sci.*, **63**, 309–324.
- Heymsfield, G. M., and Coauthors, 1996: The EDOP radar system on the high-altitude NASA ER-2 aircraft. *J. Atmos. Oceanic Technol.*, **13**, 795–809.
- Houze, R. A., Jr., 1984: *Cloud Dynamics*. Academic Press, 573 pp.
- Hudson, J., and J. Simpson, 2002: Cloud condensation nuclei measurements in tropical cyclones. *Eos, Trans. Amer. Geophys. Union*, **83** (Spring Meeting Suppl.), Abstract A41D. [Available online at http://www.agu.org/meetings/sm02/sm02-pdf/sm02_A41D.pdf.]
- Jorgensen, D. P., E. J. Zipser, and M. A. LeMone, 1985: Vertical motions in intense hurricanes. *J. Atmos. Sci.*, **42**, 839–856.
- Karyampudi, V. M., G. S. Lai, and J. Manobianco, 1998: Impact of initial conditions, rainfall assimilation, and cumulus parameterization on simulations of Hurricane Florence (1988). *Mon. Wea. Rev.*, **126**, 3077–3101.
- Krishnamurti, T. N., W. Han, B. Jha, and H. S. Bedi, 1998: Numerical prediction of Hurricane Opal. *Mon. Wea. Rev.*, **126**, 1347–1363.
- Lin, Y.-L., R. D. Farley, and H. D. Orville, 1983: Bulk parameterization of the snow field in a cloud model. *J. Climate Appl. Meteor.*, **22**, 1065–1092.
- Liu, Y., D.-L. Zhang, and M. K. Yau, 1997: A multiscale numerical study of Hurricane Andrew (1992). Part I: Explicit simulation and verification. *Mon. Wea. Rev.*, **125**, 3073–3093.
- , —, and —, 1999: A multiscale numerical study of Hurricane Andrew (1992). Part II: Kinematics and inner-core structures. *Mon. Wea. Rev.*, **127**, 2597–2620.
- Lord, S. J., and J. M. Lord, 1988: Vertical velocity structure in an axisymmetric, nonhydrostatic tropical cyclone model. *J. Atmos. Sci.*, **45**, 1453–1461.
- , H. E. Willoughby, and J. M. Piotrowicz, 1984: Role of a parameterized ice-phase microphysics in an axisymmetric, nonhydrostatic tropical cyclone model. *J. Atmos. Sci.*, **41**, 2836–2848.

- Marks, F. D., Jr., 1985: Evolution and structure of precipitation in Hurricane Allen (1980). *Mon. Wea. Rev.*, **113**, 909–930.
- , and R. A. Houze Jr., 1987: Inner core structure of Hurricane Alicia from airborne Doppler radar observations. *J. Atmos. Sci.*, **44**, 1296–1317.
- McCumber, M., W.-K. Tao, J. Simpson, R. Penc, and S.-T. Soong, 1991: Comparison of ice-phase microphysical parameterization schemes using numerical simulations of tropical convection. *J. Appl. Meteor.*, **30**, 985–1004.
- McFarquhar, G. M., and R. A. Black, 2004: Observations of particle size and phase in tropical cyclones: Implications for mesoscale modeling of microphysical processes. *J. Atmos. Sci.*, **61**, 422–439.
- Pasch, R. J., and D. P. Brown, cited 2002: Tropical cyclone report: Hurricane Erin: Hurricane Erin, 1–15 September 2001. National Hurricane Center Report. [Available online at <http://www.nhc.noaa.gov/2001erin.html>.]
- Reisner, J., R. M. Rasmussen, and R. T. Bruintjes, 1998: Explicit forecasting of supercooled liquid water in winter storms using the MM5 mesoscale model. *Quart. J. Roy. Meteor. Soc.*, **124**, 1071–1107.
- Rogers, R., M. Black, S. Chen, and R. Black, 2004: Evaluating microphysical parameterization schemes for use in hurricane environments. Preprints, *26th Conf. on Hurricanes and Tropical Meteorology*, Miami, FL, Amer. Meteor. Soc., CD-ROM, 13 C.6.
- Smith, P. L., 1984: Equivalent radar reflectivity factors for snow and ice particles. *J. Appl. Meteor.*, **23**, 1258–1260.
- Spencer, R. W., R. E. Hood, F. J. LaFontaine, E. A. Smith, R. Platt, J. Galliano, V. L. Griffin, and E. Lobl, 1994: High-resolution imaging of rain systems with the advanced microwave precipitation radiometer. *J. Atmos. Oceanic Technol.*, **11**, 849–857.
- Stoelinga, M. T., 2005: Simulated equivalent reflectivity factors as currently formulated in RIP: Description and possible improvements. 5 pp. [Available online at http://www.atmos.washington.edu/~stoelinga/RIP_sum_ref.pdf.]
- Tao, W.-K., and J. Simpson, 1993: Goddard Cumulus Ensemble Model. Part I: Model description. *Terr. Atmos. Oceanic Sci.*, **4**, 35–72.
- Vernoy, M. W., and D. Kyle, 2002: *Behavioral Statistics in Action*. McGraw-Hill, 527 pp.
- Willoughby, H. E., H.-L. Jin, S. J. Lord, and J. M. Piotrowicz, 1984: Hurricane structure and evolution as simulated by an axisymmetric, nonhydrostatic numerical model. *J. Atmos. Sci.*, **41**, 1169–1186.
- Wu, L., S. A. Braun, J. Halverson, and G. Heymsfield, 2006: A numerical study of Hurricane Erin (2001). Part I: Model verification and storm evolution. *J. Atmos. Sci.*, **63**, 65–86.
- Yuter, S. E., and R. A. Houze, 1995: Three-dimensional kinematic and microphysical evolution of Florida cumulonimbus. Part II: Frequency distributions of vertical velocity, reflectivity, and differential reflectivity. *Mon. Wea. Rev.*, **123**, 1941–1963.